An Immuno-Epidemiological Model of Foot-and-Mouth Disease (FMD) in African Buffalo Population with Carrier Transmission

Summer Atkins[1], Hayriye Gulbudak[2*], J. Shane Welker[3], Houston Smith[1,4]

[1]Department of Mathematics, Louisiana State University, 303 Lockett Hall, 175 Field House Drive, Louisiana State University, Baton Rouge, LA, 70803, USA.
[2*]Mathematics Department, University of Louisiana at Lafayette, 217 Maxim Doucet Hall, 1401 Johnston Street, Lafayette, LA, 70503, USA.
[3]Department of Mathematics, University of North Alabama, Stevens Hall, Room 110C, Florence, AL, 35632, USA.
[4]Undergraduate Student.

*Corresponding author(s). E-mail(s): hayriye.gulbudak@louisiana.edu;
Contributing authors: srnatkins@lsu.edu; jwelker1@una.edu; hsmi137@lsu.edu;

Abstract

Foot-and-mouth disease (FMD) is a highly contagious disease that spreads among cloven-hoofed animals. Although not deadly, FMD can cause major delays in meat and dairy production. One major concern is that the foot-and-mouth disease virus (FMDV) can persist in African buffalo hosts as natural reservoirs for long periods of time, causing the pathogens to reemerge in susceptible populations. In this paper, we present a novel immuno-epidemiological model of FMD in African buffalo host population. Upon infection, the hosts can undergo two phases, namely the acute and the carrier stages. In our model, we divide the infectious population based upon these two stages so that we can dynamically capture the immunological characteristics of both phases of the disease to better understand the carrier's role in transmission. We first define the within-host viral-immune kinetics dependent epidemiological basic reproduction number $\boldsymbol{\mathcal{R}_0}$ and show that it is a threshold condition for the local stability of the disease-free equilibrium and existence of the endemic equilibrium. We also analytically show that

the system always displays forward bifurcation with respect to between-host epidemic parameters. Later, by using sensitivity analysis (SA) approach developed for multi-scale models, we assess the impact of the acute infection and carrier phase immunological parameters on $\boldsymbol{\mathcal{R}_0}$. Interestingly, our numerical results show that the within-carrier infected host immune kinetics parameters and the susceptible individual recruitment rates play significant roles in disease persistence, which are consistent with experimental and field studies.

Keywords: Foot-and-mouth disease (FMD), multi-scale modeling, carrier transmission, stability analysis, carrier phase, within-carrier host virus-immune kinetics.

MSC Classification: 92D30

1 Introduction

The foot-and-mouth disease virus (FMDV) is a fast-evolving and fast-transmitting pathogen that can infect a plethora of cloven-hoofed species, including domestic livestock and numerous wildlife species (Garabed et al., 2020). The transmission of FMDV can be through both direct and indirect contact between animals, through fomites, and even through airborne spread under certain atmospheric conditions (Gloster, 1983). Although the foot-and-mouth disease (FMD) is not deadly, outbreaks of FMD can be devastating to agriculture and wildlife economies. The economic impact of FMD is largely due to control measures (*e.g.* restricting market access for livestock and livestock products from affected areas, quarantining of infected/exposed animals, culling of infected animals, and even mass culling of contagious premises) that are used for curtailing the spread of the disease among livestock populations (Shikumwifa, 2022). FMD remains a serious economic problem in South African regions. The main obstacle in disease eradication is the presence of large numbers of infected African buffalo, as they are able to transfer FMDV to livestock with serotypes South African Territories (SAT) 1, 2, and 3 (Shikumwifa, 2022; Michel and Bengis, 2012). FMD infected buffalo can undergo two stages of the disease: the primary infection stage, which is called the acute phase, and a secondary stage, which is commonly called the carrier phase because they serve as carriers to the disease. In this paper, we construct an immuno-epidemiological model of FMD in the buffalo population which captures the immunological characteristics of the carrier phase to better understand how carrier infection contribute to the spread of the disease.

In the acute phase, the virus is found in both the bloodstream and in the tonsils. Experimental studies show that the viral clearance in the bloodstream is obtained within 30 days post infection; however, the viral load may or may not clear in the tonsils during that time frame (Perez-Martin et al., 2022). If the pathogen load in the tonsils does clear within 30 days, then the individual is considered to be recovered and only undergoes the acute stage of the disease. Otherwise, the individual enters the secondary stage of the disease and is classified as being a carrier. The duration of the carrier phase can last from months to even years (Stenfeldt C, 2020; Shikumwifa, 2022).

Understanding the persistence of FMDV in host populations and how the role of carrier transmission contributes to disease persistence is ultimately a multi-scale problem in which both immunological and epidemiological scales need to be investigated (Stenfeldt C, 2020; Garabed et al., 2020; Jolles et al., 2021). In prior works, deterministic models of FMD have been used for understanding the spread of FMD (Pech and McIlroy, 1990; Chowell et al., 2006), the ways of controlling the spread of FMD (Gashirai et al., 2020; Shikumwifa, 2022), and the persistence of FMDV among livestock and reservoir populations (Hayer et al., 2018; McLachlan et al., 2019). With regard to analyzing FMD at the immunological scale, there have been some works (Howey et al., 2009, 2012; Macdonald et al., 2022) in which systems of ordinary differential equations (ODEs) were constructed to model the viral and immunological dynamics of FMDV. Howey et al. (2009) constructed a within-host model to capture the viral dynamics of needle-infected pigs and found a trend in which the higher the initial dose the earlier the development of viral detection. In another work, Howey et al. (2012) constructed a within-host model consisting of eight compartments to investigate viral dynamics of FMDV in cattle and found that the within-host model parameters fitted varied from host to host. They assert that a better understanding of the within-host dynamics also provides insights into the dynamics of infectiousness and the transmission of the virus to new host. In prior work (Macdonald et al., 2022), we also construct a within-host model to capture the viral and immunological dynamics of FMDV in African buffalo during the acute phase. The model was fitted to time series data corresponding buffalo who were infected with one of three strains (SAT1, SAT2, and SAT3) of FMDV. In analyzing this model across-scale linkages, we find that the viral replication rate in the host highly correlates with the transmission rate on the population scale and that the adaptive immune response activation rate highly correlates with the acute-infection period, making both within-host viral growth rate and the adaptive immune reponse activation rate crucial parameters in disease dynamics. We find this work as being a stepping stone to multi-scale modeling of FMD in which the within-host dynamics of FMDV can be rigorously linked to epidemiological scales.

To the best of our knowledge, there have not been any multiscale modeling approach applied to FMD that link the immunological dynamics to the population dynamics. The majority of the literature associated with modeling of FMD focus on spatial scales of interest (Bradhurst et al., 2015; Ferguson et al., 2001; Hayama et al., 2013; Keeling et al., 2001; Tildesley et al., 2006; Michael J. Tildesley and Woolhouse, 2009). These studies sought to parameterize models that predict disease spread at farm to regional and national scales in order to best evaluate interventions used for limiting transmission and the risk of major epidemics (note the majority of these models are stochastic). However, there have been works in which carrier transmission is investigated (Shikumwifa, 2022; Thomson et al., 1992; Juleff et al., 2008; Maree et al., 2016; Jolles et al., 2021; McLachlan et al., 2019). In this paper, we present an immuno-epidemiological model of FMD in African buffalo (in particular serotype SAT1) to investigate how the within-host viral and immune kinetics affect the spread of the disease. In particular, we investigate the role of carrier transmission in the context of FMDV disease ecology. We couple an age-structured epidemiological system (where infection age corresponds to time-since-host infection) with two within-host

immunological models representing different phases, namely the acute and carrier. We first define the within-host viral-immune kinetics dependent epidemiological basic reproduction number $\mathcal{R}_0$ and show that it is a threshold condition for the local stability of the disease-free equilibrium and existence of the endemic equilibrium. We also analytically show that the system always displays forward bifurcation with respect to between-host epidemic parameters. Numerical results suggest that the presence of carrier infected individuals and the birth of new susceptible individuals are the driving influences of disease persistence, which aligns with what was observed in Jolles et al. (2021). Lastly, we use a sensitivity analysis approach (as developed in Gulbudak et al. (2022)), to investigate the impact of the within-host viral and immune kinetics (during both stages of the disease) on the disease outcomes. Interestingly, numerical results suggest that the adaptive immune response activation rate during the acute phase has the largest impact on the epidemiological basic reproduction number (10).

The paper is organized as follows. In Section 2, we first present two immunological models of FMDV, representing the virus-immune response dynamics during the acute and carrier phases. We analyze the within-carrier host immune model. We then present the age-since-infection structured epidemiological between-host model. In Section 3, we provide the threshold and bifurcation analysis of the multiscale model. In Section 4, we present numerical simulations of the model and discuss the epidemiological implications. In Section 5, we use a sensitivity analysis approach to investigate the impact of the within-host parameters (in particular carrier transmission parameters) on the epidemiological quantities. In the last section, we summarize our results and give the conclusion.

2 An immuno-epidemiological model of FMD with acute and carrier phases

In this section, we present our immuno-epidemiological model that captures the disease spread of foot-and-mouth disease among African buffalo on two scales (namely the immunological and epidemiological). We first discuss our within-host model, which is initially presented in Macdonald et al. (2022), modeling the virus and immune dynamics of the FMDV infected buffalo during the acute phase. Next, we present the within-host model for carrier-infected buffalo and formulate an age-since-infection structured PDE epidemic model. Lastly, we link these within-host models to a population-scale epidemiological PDE model.

2.1 Immunological model of an acute-infected individual

Here, we introduce the within-host viral immune kinetics model describing the acute infection stage of infected host (formulated first in our prior work Macdonald et al. (2022)). The model considers the interactions between the innate immune response, $I_A(\tau)$, the virus in the bloodstream, $P(\tau)$, and the adaptive immune response $A(\tau)$, where τ refers to the time since infection within a host (in days). The model is given in (1) with initial conditions (densities) $I_A(\tau_0) = I_{A0},\ P(\tau_0) = P_0$, and $A(\tau_0) = A_0$. The innate response is assumed to clear the pathogen at a rate θ. We assume that the adaptive response, which is mediated by neutralizing antibodies produced by the

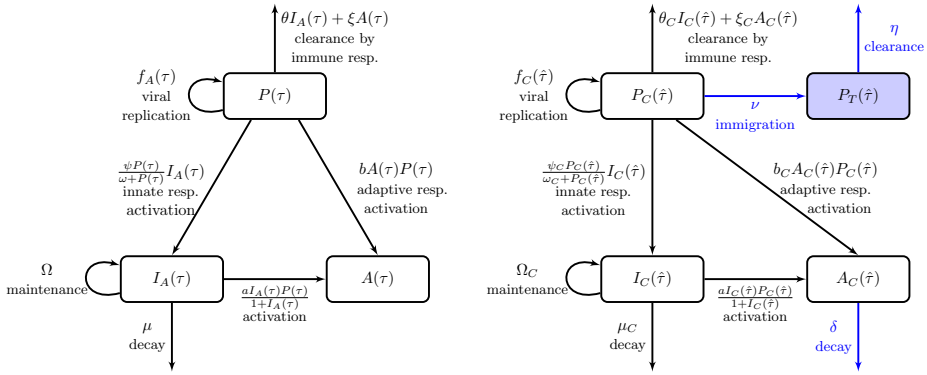

Fig. 1: Flowcharts of the within-host dynamics of the acute infectious individual (left) and the carrier infected individual (right), with $f_A(\tau) = r_A P(\tau)[1 - P(\tau)/K_A]$ and $f_C(\hat{\tau}) = r_C P_C(\hat{\tau})[1 - P_C(\hat{\tau})/K_C]$. Note that only a proportion of acute-infected individuals undergo a carrier phase.

host B cells, clears the pathogen at rate ξ. We assume that the adaptive immune response is activated based upon two processes. One way is independent of the innate response which is represented by $bA(\tau)P(\tau)$ with activation rate b. While the other is due to the alarm signals generated by the innate response, which is represented by $aI(\tau)P(\tau)/(1 + I(\tau))$, with activation rate a and with half saturating constant scaled to 1. With regard to the pathogen, logistic growth is considered with a replication rate of r_A and a within-host viral carrying capacity in the absence of adaptive immune response, K_A. Innate response effectors are always present at a maintenance level Ω/μ, where Ω is the maintenance level and μ is the immune response decay rate. When the virus invades, the innate response get activated as a saturating function of virus density with a maximum rate of ψ and a half saturation constant ω. The within-host acute infection model is as follows:

$$
\begin{aligned}
\frac{\mathrm{d}I_A}{\mathrm{d}\tau} &= \Omega + \frac{\psi P(\tau)}{\omega + P(\tau)} I_A(\tau) - \mu I_A(\tau) \\
\frac{\mathrm{d}P}{\mathrm{d}\tau} &= \left[r_A \left(1 - \frac{P(\tau)}{K_A} \right) - \theta I_A(\tau) - \xi A(\tau) \right] P(\tau) \\
\frac{\mathrm{d}A}{\mathrm{d}\tau} &= \left[a \frac{I(\tau)}{1 + I(\tau)} + bA(\tau) \right] P(\tau).
\end{aligned}
\tag{1}
$$

A schematic diagram of the above model is presented on the left-hand side of Figure 1.

A detailed analysis of the immunological model is presented in Macdonald et al. (2022). In particular, the following result is established:

Theorem 2.1 (Macdonald et al. (2022)). *If $I_{A0} > 0$ or $A_0 > 0$, then the pathogen (within the host) eventually clears, i.e.,*

$$\lim_{\tau \to \infty} P(\tau) = 0.$$

Subsequently, the innate immune response antibodies decay and the adaptive immune response antibodies increase to a steady state solution, respectively, i.e.,

$$\lim_{\tau \to \infty} I_A(\tau) = \Omega/\mu$$

and

$$\lim_{\tau \to \infty} A(\tau) = A^+,$$

where $A^+ > 0$ depends on the initial condition; i.e. $A^+ = z(P_0, I_{A0}, A_0)$.

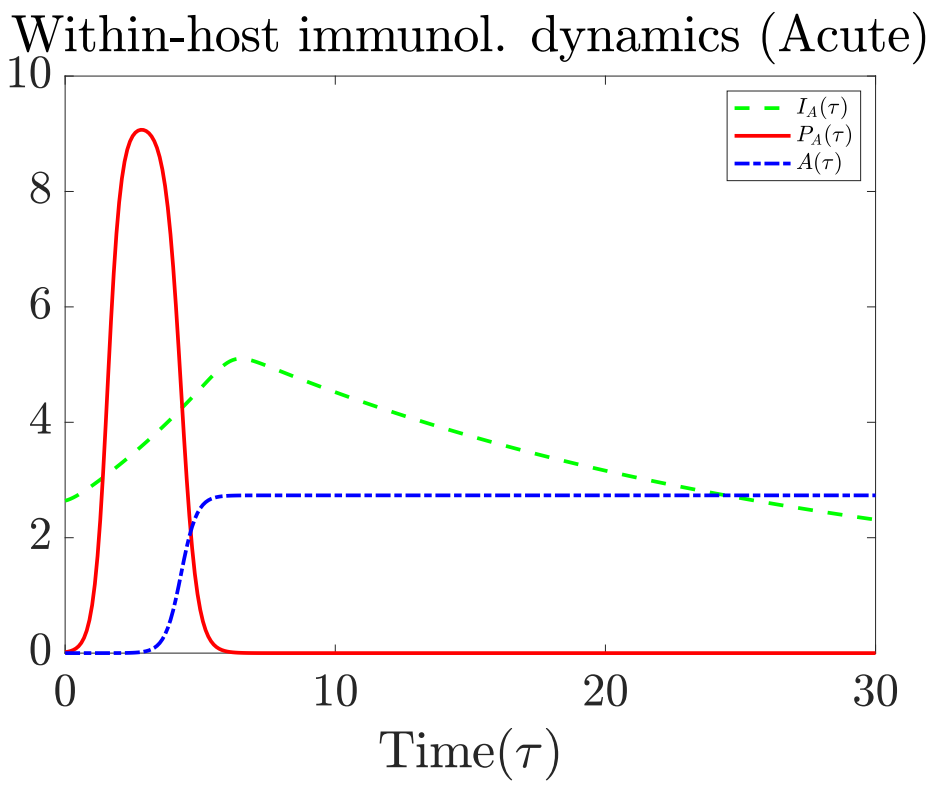

Fig. 2: Within-host pathogen-immune response antibody dynamics of an infectious individual during the acute phase. Parameter values used are given in Table 3.

Parameter and state variable descriptions of system (1) are given in Table 3 and Table 4. The acute infection model parameters are estimated in our prior work Macdonald et al. (2022).

Figure 2 displays a time-dependent solution of the within-acute model (1) (with parameter value settings given in Table 3), which was numerically obtained through MATLAB's ODE solver, ode45. Notice that the pathogen in the bloodstream peaks around day 3. Also the time τ in which $P_A(\tau) < 10^{-4}$ (the lowest viral density threshold for assuming pathogen clearance) is approximately 7.7 days. This is reasonably close to estimates obtained from Jolles et al. (2021), which approximated the acute infection period at 5.7 days. Once the pathogen has been cleared from the bloodstream, the individual either recovers or progresses to the carrier infection stage. The latter case is due to the pathogen persisting in the tonsils.

2.2 Immunological model of a carrier-infected individual

Here, we formulate an immunological model, describing the within-carrier host virus-immune response dynamics. Similar to the within-host model for the acutely infectious individuals, the model variables are the innate immune response, $I_C(\hat{\tau})$, the viral load in the bloodstream, $P_C(\hat{\tau})$, and the adaptive immune response, $A_C(\hat{\tau})$ with the independent time variable $\hat{\tau}$, referring the time passed after infection. Additionally, the within-carrier model has a compartment describing the pathogen load in the tonsils, $P_T(\hat{\tau})$. Regarding FMD infection, the pathogen resides in the tonsils due to dendritic cell transportation, and an FMD-infected buffalo becomes a carrier when the pathogen clears in the bloodstream but remains in the tonsils for an extended period of time.

For FMD, unlike many other pathogens, dendritic cells pick up some complete copies of virus instead of only viral fragments. Consequently, we assume pathogen enters the tonsils at rate $\nu P_C(\hat{\tau})(1 - P_T(\hat{\tau})/K_T)$. The parameter K_T corresponds to a viral carrying capacity in the tonsils. We also assume the pathogen in the tonsils exits at rate η, at which point it may be transported to mucosal cells allowing for the possibility of carrier transmission. Since the carrier phase is significantly longer than the acute phase, we add a decay rate for the adaptive immune response, δ, to the model. We also assume that the adaptive response is activated through two processes: (1) the adaptive response is activated independent of the innate response at a rate b_C, and (2) interferons acting as part of the innate response send alarm signals for adaptive immune response production. Hence an activation rate $aI_C(\tau)/(1 + I_C(\tau))$ is considered, but like the within-host acute model, we set $a = 0$. We assume that innate immune response effectors are always present at a maintenance level Ω_C in the absence of the virus. The innate immune response is activated at a maximum rate ψ_C with half-saturation constant in terms of the viral load ω_C, and decays at a rate μ_C.

The model is given in (2) with initial conditions (densities) being $P_T(\hat{\tau}_0) = P_{T0}$, $I_C(\hat{\tau}_0) = I_{C0}$, $P_C(\hat{\tau}_0) = P_{C0}$, and $A_C(\hat{\tau}_0) = A_{C0}$.

$$\begin{aligned}
\frac{\mathrm{d}P_T(\hat{\tau})}{\mathrm{d}\hat{\tau}} &= \nu P_C(\hat{\tau})\left[1 - \frac{P_T(\hat{\tau})}{K_T}\right] - \eta P_T(\hat{\tau}) \\
\frac{\mathrm{d}I_C(\hat{\tau})}{\mathrm{d}\hat{\tau}} &= \Omega_C + \frac{\psi_C P_C(\hat{\tau})}{\omega_C + P_C(\hat{\tau})} I_C(\hat{\tau}) - \mu_C I_C(\hat{\tau}) \\
\frac{\mathrm{d}P_C(\hat{\tau})}{\mathrm{d}\hat{\tau}} &= \left[r_C\left(1 - \frac{P_C(\hat{\tau})}{K_C}\right) - \theta_C I_C(\hat{\tau}) - \xi_C A_C(\hat{\tau}) - \nu\right] P_C(\hat{\tau}) \\
\frac{\mathrm{d}A_c(\hat{\tau})}{\mathrm{d}\hat{\tau}} &= \left[a\frac{I_C(\hat{\tau})}{1 + I_C(\hat{\tau})} + b_C A_C(\hat{\tau})\right] P_C(\hat{\tau}) - \delta A_C(\hat{\tau})
\end{aligned} \tag{2}$$

On the right-hand side of Figure 1, a schematic diagram of the within-host model for the carrier stage is provided.

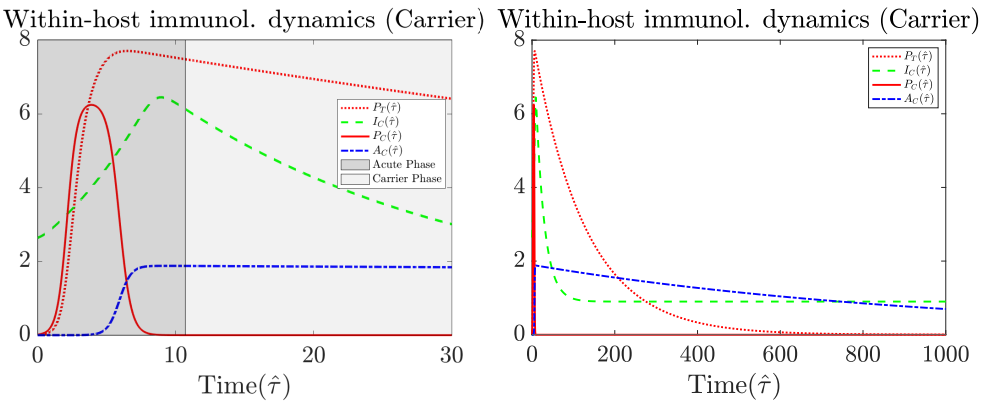

(a) The carrier-infected host's viral and immune response.

(b) Within-carrier host dynamics over a longer time frame

Fig. 3: The within-host dynamics of an infected buffalo during the carrier stage. Parameter values used are given in Table 3. Note that carrier-infected host experience an acute phase (the dark grey shaded region in Subfigure(a)). Subfigure(b) presents the same dynamics but over a longer time frame, illustrating that the pathogen load in the tonsils starts to become negligible around 500 days.

Similar to the within-host acute model (1), logistic growth is assumed for the pathogen in the bloodstream with a replication rate r_C and viral carrying capacity in the absence of the adaptive immune response K_C. Additionally, we assume that the innate response clears the pathogen at rate θ_C and the adaptive immune response clears the pathogen at rate ξ_C due to neutralizing antibodies produced by host B cells. In regards to the parameter settings, we set the value for Ω_C, ψ_C, ω_C, μ_C, r_C, K_C, θ_C, ξ_C, b_C equal to Ω, ψ, ω, μ, r_A, K, θ, ξ, and b (respectively), which are the

parameter values that correspond to the same rates in the acute model. The data that we use to calibrate the remaining parameters come from experiments generated in Jolles et al. (2021). In Jolles et al. (2021), African buffalo were needle infected with different strains (SAT1, SAT2, and SAT3) and were analyzed over a span of 6.5 months post infection. We use the tonsil swab data collected from four of the SAT1 needle-infected individuals who became carriers.

A detailed analysis of the immunological model (2) is presented below and proofs are provided in the Appendix A. It is worth noting that system (2) (with $a = 0$) possesses a pathogen-free equilibrium (PFE) and up to two pathogen-persisting equilibria.

Before presenting the analytical results, we define the immunological basic reproduction number

$$\mathscr{R}_0 = \frac{r_C}{\theta_C \frac{\Omega_C}{\mu_C} + \nu}. \tag{3}$$

The immunological reproduction number, $\mathscr{R}_0$, gives the number of secondary viral particles that one viral particle will produce in the bloodstream (before the adaptive immune response is mounted). Next we establish the following result:

Theorem 2.1. *The pathogen-free equilibrium*

$$\mathcal{E}_0 = \left(0,\ \frac{\Omega_C}{\mu_C},\ 0,\ 0\right),$$

which always exists, is locally asymptotically stable when

$$\mathscr{R}_0 < 1$$

and unstable when

$$\mathscr{R}_0 > 1.$$

Proof. See the proof in Appendix A.1. □

In the absence of adaptive immune response, the system (2) also has a pathogen-persisting boundary equilibrium

$$\mathcal{E}_1^* = (P_T^*,\ I_C^*,\ P_C^*, 0),$$

where

$$\begin{aligned} P_T^* &= \frac{\nu P_C^*}{\frac{\nu P_C^*}{K_T} + \eta} = \frac{\nu K_T P_C^*}{\nu P_C^* + \eta K_T}, \\ I_C^* &= \frac{\Omega_C(\omega_C + P_C^*)}{\mu_C(\omega_C + P_C^*) - \psi_C P_C^*} = \frac{\Omega_C}{\mu_C}\left(\frac{1}{1 - \frac{\psi_C P_C^*}{\mu_C(\omega_C + P_C^*)}}\right), \end{aligned} \tag{4}$$

and P_C^* is the positive root to the following quadratic equation:

$$0 = f(P_C) = \hat{A}_2 (P_C)^2 + \hat{A}_1 P_C + \hat{A}_0, \tag{5}$$

where

$$\begin{aligned}
\hat{A}_2 &= -r_C(\mu_C - \psi_C),\\
\hat{A}_1 &= K_C\left[(r_C-\nu)(\mu_C-\psi_C) - \theta_C\Omega_C\right] - r_C\mu_C\omega_C,\\
\hat{A}_0 &= K_C\omega_C[(r_C-\nu)\mu_C - \theta_C\Omega_C].
\end{aligned}$$

Note that we can rewrite the coefficients for $\hat{A}_1$ and $\hat{A}_0$ as follows:

$$\begin{aligned}
\hat{A}_1 &= K_C\left[r_C\mu_C\left(1-\frac{1}{\mathscr{R}_0}\right) - \psi_C(r_C-\nu)\right] - r_C\mu_C\omega_C\\
\hat{A}_0 &= r_C\omega_C\mu_C K_C\left(1-\frac{1}{\mathscr{R}_0}\right).
\end{aligned}$$

Theorem 2.2. *If one of the two following conditions below holds:*

1. $\mathscr{R}_0 > 1$ *and* $\mu_C > \psi_C$.
2. $\mathscr{R}_0 > 1$, $\mu_C < \psi_C$, *and the discriminant of the quadratic polynomial* $f(P_C)$, $\hat{A}_1^2 - 4\hat{A}_0\hat{A}_2$, *is positive,*

then there exists a unique pathogen-persisting boundary equilibrium $\mathcal{E}_1^*$. *Moreover if* $P_C^* < \frac{\delta}{b_C}$, *then the pathogen persisting boundary equilibrium is locally asymptotically stable.*

Proof. See the proof in Appendix A.2. □

In addition, the system (2) has a pathogen-persisting interior equilibrium

$$\mathcal{E}_2^* = (P_T^*,\ I_C^*,\ P_C^*,\ A_C^*),$$

where

$$\begin{aligned}
P_T^* &= \frac{\nu K_T P_C^*}{\nu P_C^* + \eta K_T} = \frac{\nu K_T \delta}{\nu\delta + \eta b_C K_T},\\
I_C^* &= \frac{\Omega_C(\omega_C + P_C^*)}{\mu_C(\omega_C+P_C^*) - \psi_C P_C^*} = \frac{\Omega_C}{\mu_C}\left(\frac{1}{1-\frac{\psi_C P_C^*}{\mu_C(\omega_C+P_C^*)}}\right) = \frac{\Omega_C}{\mu_C}\left(\frac{1}{1-\mathscr{R}_1}\right),\\
P_C^* &= \frac{\delta}{b_C},\\
A_C^* &= \frac{1}{\xi_C}\left[r_C\left(1-\frac{P_C^*}{K_C}\right) - \frac{\theta_C\Omega_C(\omega_C+P_C^*)}{\mu_C(\omega_C+P_C^*)-\psi_C P_C^*} - \nu\right]\\
&= \frac{1}{\xi_C}\left(\frac{\theta_C\Omega_C}{\mu_C}\left(\frac{1}{1-\mathscr{R}_1}\right) + \nu\right)(\mathscr{R}_2 - 1),
\end{aligned} \tag{6}$$

where

$$\mathscr{R}_1 = \frac{\psi_C\frac{\delta}{b_C}}{\mu_C\left(\omega_C + \frac{\delta}{b_C}\right)} \text{ and } \mathscr{R}_2 = \frac{r_C\left(1-\frac{\frac{\delta}{b_C}}{K_C}\right)}{\frac{\theta_C\Omega_C}{\mu_C}\left(\frac{1}{1-\mathscr{R}_1}\right)+\nu}.$$

We establish the following analytical result:

Theorem 2.3. *The pathogen-persisting interior equilibrium,* $\mathcal{E}_2^* = (P_T^*,\ I_C^*,\ P_C^*,\ A_C^*)$, *exists and is locally asymptotically stable if*

$$\mathscr{R}_1 < 1 \text{ and } \mathscr{R}_2 > 1. \tag{7}$$

Proof. See the proof in Appendix A.3. □

It is worth mentioning that the two inequalities in (7) imply that we are in a parameter setting in which $\mathscr{R}_0 > 1$ (i.e. the pathogen-free equilibrium is unstable).

Reproduction Numbers	
Pathogen-free	$\mathscr{R}_0 = \dfrac{r_C}{\theta_C \frac{\Omega_C}{\mu_C} + \nu}$
Innate response	$\mathscr{R}_1 = \dfrac{\psi_C \frac{\delta}{b_C}}{\mu_C \left(\omega_C + \frac{\delta}{b_C}\right)}$
Pathogen-persisting boundary	$\mathscr{R}_2 = \dfrac{r_C \left(1 - \frac{\frac{\delta}{b_C}}{K_C}\right)}{\frac{\theta_C \Omega_C}{\mu_C}\left(\frac{1}{1-\mathscr{R}_1}\right) + \nu}$

Table 1: Threshold quantities for the within-carrier system.

Equilibrium	Notation	P_T^*	I_C^*	P_C^*	A_C^*	Stability Condition
Pathogen-free	$\mathcal{E}_0$	0	$\frac{\Omega_C}{\mu_C}$	0	0	$\mathscr{R}_0 < 1$
Boundary pathogen-persisting	$\mathcal{E}_1^*$	$P_{T2}^{\ddagger}$	$I_{C2}^{\ddagger}$	$P_{C2}^{\ddagger}$	0	Exists$^{(*)}$ & $P_{C2}^{\ddagger} < \frac{\delta}{b_C}$
Interior pathogen-persisting	$\mathcal{E}_2^*$	$P_{T1}^{\dagger}$	$I_{C1}^{\dagger}$	$P_{C1}^{\dagger}$	$A_{C1}^{\dagger}$	$\mathscr{R}_1 < 1$ & $\mathscr{R}_2 > 1$

Table 2: Equilibria and local stability for the within-carrier system
$^{(*)}$Conditions stated in Theorem 2.2.
‡Equilibrium expressions given in (4) and (5).
† Equilibrium expressions found in (6).

Figure 3a displays the solution of the system (2) with parameter settings given in Table 3. Note that the darker gray region represents the acute phase of the infected individual while the lighter gray region is the carrier phase. In Figure 3b, we see the same plot of the carrier phase over the first 750 days. We only consider the first 750 days since the data (Perez-Martin et al., 2022) used for parameterization involve juvenile buffalo who are only being observed for one to three years. The majority of the parameter values are obtained from Macdonald et al. (2022). However, based

upon these parameter values, the solution to the dynamical system converges to the pathogen-persisting interior equilibrium, with $\mathcal{E}_2^* \approx (0.4011, 1.8117, 0.0027, 1.0293)$. Figure 11 in D illustrates that the carrier individual eventually experiences multiple instances of viral relapse, where the solution converges to the pathogen-persisting interior equilibrium.

2.3 The epidemiological model

At the *population scale*, we consider a time-since-infection structured epidemic model with the acute and carrier stages of infection. In the model, the variables $S(t)$, $I(t)$, $C(t)$, $R(t)$, and $M(t)$ represent the numbers of *susceptible*, *acute-infected*, *carrier-infected*, *recovered*, and the *maternally immune* host population, respectively. Let $i(\tau, t)$ represents the acute-infected host density with time-since-host infection τ at time t. Let $c(\hat{\tau}, t)$ represent the carrier infected-host density, where $\hat{\tau}$ is the time since becoming a carrier. The total number of infected individuals during the acute phase at time t is

$$I(t) = \int_0^\infty i(\tau, t)\,\mathrm{d}\tau.$$

Similarly, the number of infected individuals that are carriers at time t is

$$C(t) = \int_0^\infty c(\hat{\tau}, t)\,\mathrm{d}\hat{\tau}.$$

The full model of the between-host system is as follows:

$$\begin{aligned}
\frac{\mathrm{d}M(t)}{\mathrm{d}t} &= \Lambda\left(R(t) + \int_0^\infty c(\hat{\tau}, t)\,\mathrm{d}\hat{\tau}\right)\left(1 - \frac{N(t)}{K}\right) - dM(t) - wM(t),\\
\frac{\mathrm{d}S(t)}{\mathrm{d}t} &= \Lambda\left(S(t) + \int_0^\infty i(\tau, t)\,\mathrm{d}\tau\right)\left(1 - \frac{N(t)}{K}\right) + wM(t)\\
&\quad - S(t)\left(\int_0^\infty \beta(\tau) i(\tau, t)\,\mathrm{d}\tau + \int_0^\infty \beta_C(\hat{\tau}) c(\hat{\tau}, t)\,\mathrm{d}\hat{\tau}\right) - dS(t),\\
\frac{\partial i}{\partial \tau} + \frac{\partial i}{\partial t} &= -(\gamma(\tau) + d)\; i(\tau, t),\\
i(0, t) &= S(t)\left(\int_0^\infty \beta(\tau) i(\tau, t)\,\mathrm{d}\tau + \int_0^\infty \beta_C(\hat{\tau}) c(\hat{\tau}, t)\,\mathrm{d}\hat{\tau}\right),\\
\frac{\mathrm{d}R(t)}{\mathrm{d}t} &= (1 - \rho)\int_0^\infty \gamma(\tau) i(\tau, t)\,\mathrm{d}\tau + \int_0^\infty \alpha(\hat{\tau}) c(\hat{\tau}, t)\,\mathrm{d}\hat{\tau} - dR(t),\\
\frac{\partial c}{\partial \hat{\tau}} + \frac{\partial c}{\partial t} &= -(\alpha(\hat{\tau}) + d)\; c(\hat{\tau}, t),\\
c(0, t) &= \rho \int_0^\infty \gamma(\tau) i(\tau, t)\,\mathrm{d}\tau.
\end{aligned} \tag{8}$$

Animals in the recovered (R) and carrier (C) classes give birth to individuals who enter the M class due to obtaining maternal immunity. Animals belonging to other classes give birth to new susceptible individuals. Here, $N(t)$ represents the total host population. We considered logistic growth rates, where Λ represents the per capita birth rate of buffalo and K represents the carrying capacity. Maternally

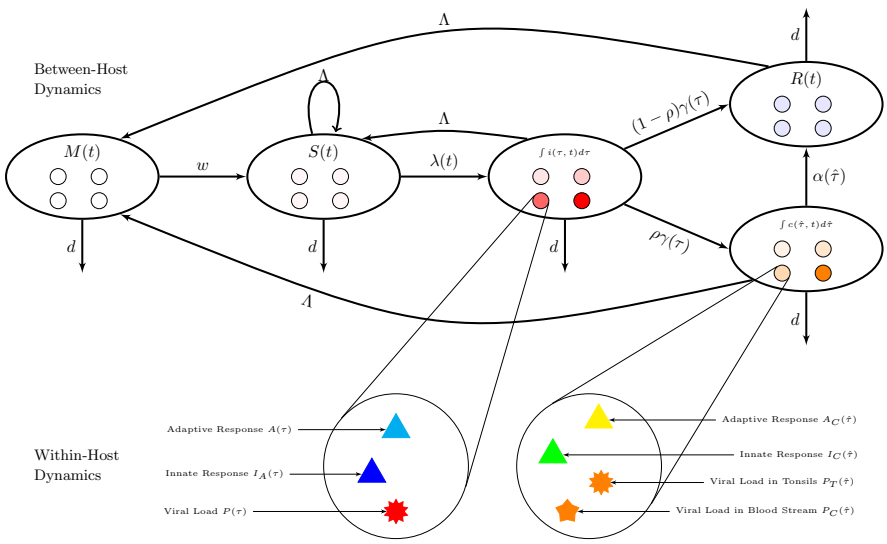

Fig. 4: Flowchart of the multi-scale model. Here $\lambda(t)$ represents the force of infection due to interacting with either an acute infected individual or a carrier infected individual.

immune individuals eventually exit the class due to their immunity waning at rate w and enter the susceptible class. We assume a density-dependent force of infection from infected individuals during the acute phase ($\int_0^\infty \beta(\tau)i(\tau,t)\,\mathrm{d}\tau$) and from carriers ($\int_0^\infty \beta_C(\hat{\tau})c(\hat{\tau},t)\,\mathrm{d}\hat{\tau}$). After successful interactions with an acutely infected or carrier infected buffalo, susceptible individuals move to infectious class $i(t,\tau)$ with a rate

$$\lambda(t) = \int_0^\infty \beta(\tau)i(\tau,t)\,\mathrm{d}\tau + \int_0^\infty \beta_C(\hat{\tau})c(\hat{\tau},t)\,\mathrm{d}\hat{\tau}.$$

Upon clearing the virus in the bloodstream, if the hosts still have virus in the tonsils, we assume these individuals become carriers and move to the carrier phase. However, not all acutely infected buffalo transition into the carrier stage. For this model, we assume that the acutely infected hosts exits at a rate $\gamma(\tau)$, which represents the clearance rate of the pathogen in the bloodstream. We let $0 < \rho < 1$ be the fraction of the acute infected individuals who become carriers, and $(1-\rho)$ is the fraction of the acute infected individuals who enter the recovered class. The carriers eventually recover at rate $\alpha(\hat{\tau})$. *In vivo* studies, along with modeling framework that we develop here, allow us to bridge the immunological and population scales by defining functional forms of epidemic parameters as functions of within-host virus immune response. For example, to bridge the scales from individual to population, the unit infectiousness and recovery rates can be formulated as functions of immunological variables as suggested by data in Handel and Rohani (2015); Fraser et al. (2014); Gulbudak et al. (2017), as

follows:

$$\begin{cases} \beta(\tau) = \dfrac{B_A P^2(\tau)}{B_0 + P^2(\tau)} \\ \gamma(\tau) = \dfrac{G_A A(\tau)}{P(\tau) + \epsilon_0} \\ \beta_C(\hat{\tau}) = \dfrac{B_C P_T^2(\hat{\tau})}{B_0 + P_T^2(\hat{\tau})} \\ \alpha(\hat{\tau}) = \dfrac{G_C A_C(\hat{\tau})}{P_C(\hat{\tau}) + P_T(\hat{\tau}) + \hat{\epsilon}_0}. \end{cases} \tag{9}$$

The transmission rate due to interaction with an acutely infected individual, $\beta(\tau)$, is modeled by a sigmoidal Hill equation of $n = 2$ that depends on the pathogen load in the bloodstream. The transmission rate due to interaction with a carrier infected individual, $\beta_C(\tau)$, is also modeled by a sigmoidal Hill equation of $n = 2$, but this function depends on the viral load in the tonsils. A Michaelis-Menton equation with $n = 1$ is considered for modeling the rate at which the viral load in the bloodstream is cleared, $\gamma(\tau)$ (Gilchrist and Sasaki, 2002; Gulbudak and Browne, 2020; Tuncer et al., 2016). The recovery rate for the carriers, $\alpha(\tau)$, has a form similar to $\gamma(\tau)$ but depends on both the viral load in the bloodstream and the tonsils. The parameters used for these linking functions are described in Table 3.

3 Equilibria and the threshold analysis

In this section, we first define the within-host virus-immune kinetics-dependent epidemiological basic reproduction number (10) and show that it is a threshold condition for both the stability of the disease-free equilibrium (DFE) and the existence of the endemic (EE) equilibrium.

The basic reproduction number $\mathcal{R}_0$ of the epidemiological model (8) is

$$\mathcal{R}_0 = \mathcal{R}_{A0} + \mathcal{R}_{C0}, \tag{10}$$

where

$$\mathcal{R}_{A0} = \hat{S}_0 \int_0^\infty \beta(\tau)\pi(\tau)\,\mathrm{d}\tau, \quad \mathcal{R}_{C0} = \hat{S}_0 \rho \int_0^\infty \gamma(\tau)\pi(\tau)\,\mathrm{d}\tau \int_0^\infty \beta_C(\hat{\tau})\pi_C(\hat{\tau})\,\mathrm{d}\hat{\tau}, \tag{11}$$

$\pi(\tau) = e^{-\int_0^\tau (\gamma(s)+d)\,\mathrm{d}s}$ gives the probability of still being in the acute phase τ days after becoming infected, and $\pi_C(\hat{\tau}) = e^{-\int_0^{\hat{\tau}} (\alpha(s)+d)\,\mathrm{d}s}$ is the probability of still being in the carrier phase $\hat{\tau}$ days after becoming a carrier.

The first term $\mathcal{R}_{A0}$ accounts for the total number of secondary cases that is produced by one infectious individual (while in the acute phase) in an entirely susceptible population. The second term $\mathcal{R}_{C0}$ accounts for the total number of secondary cases produced by one infected individual (while in the carrier phase) in a population consisting only of susceptible individuals.

Parameter	Description	Value	Source
	Immunological parameters for acute infectious		
a	Adaptive response activation rate due to innate response	0	Macdonald et al. (2022)
b	Adaptive response activation rate due to pathogen	0.37	Macdonald et al. (2022)
K_A	Viral carrying capacity	9.23	Macdonald et al. (2022)
r_A	Pathogen replication rate	4.06	Macdonald et al. (2022)
θ	Pathogen clearance rate due to innate response	0.005	fixed*
μ	Immune response decay rate	1/21.23	Macdonald et al. (2022)
ξ	Pathogen clearance rate due to adaptive response	2.72	Macdonald et al. (2022)
ψ	Max innate response activation rate	0.15	Macdonald et al. (2022)
Ω	Innate response maintenance level	0.9/21.23	Macdonald et al. (2022)
ω	Half saturation constant	$0.9 \cdot .016$	Macdonald et al. (2022)
	Immunological parameters for carriers		
a	Adaptive response activation rate due to innate response	0	Macdonald et al. (2022)
b_C	Independent adaptive response activation rate	0.37	Macdonald et al. (2022)
K_C	Viral carrying capacity absent of adaptive response	9.23	Macdonald et al. (2022)
K_T	Viral carrying capacity in tonsils	8	Calibrated
r_C	Viral growth rate	4.06	Macdonald et al. (2022)
δ	Adaptive immune response clearance rate	0.001	Calibrated
η	Decay rate of pathogen in tonsils	0.008	Calibrated
θ_C	Pathogen clearance rate due to innate response	0.005	Calibrated
μ_C	Decay rate of innate response	1/21.23	Macdonald et al. (2022)
ν	Immigration/growth rate of pathogen in tonsils	1.25	Calibrated
ξ_C	Pathogen clearance rate due to adaptive response	2.72	Macdonald et al. (2022)
ψ_C	Max innate response activation rate	0.15	Macdonald et al. (2022)
Ω_C	Innate response maintenance level	0.9/21.23	Macdonald et al. (2022)
ω_C	Half-saturation constant for innate response	$0.9 \cdot 0.016$	Macdonald et al. (2022)
	Linking function parameters		
B_0	Saturating coefficient of a Hill function	14	Calibrated
B_A	Transmission efficacy of pathogen infection (from acute)	$1.35 \cdot 10^{-5}$	Calibrated
B_C	Transmission efficacy of pathogen infection (from carrier)	$2.6 \cdot 10^{-7}$	Calibrated
G_A	Recovery (in the bloodstream) coefficient	0.0009	Calibrated
G_C	Recovery (for carriers) coefficient	0.009	Calibrated
ϵ_0	Half saturation constant in recovery rate in bloodstream	$5.9 \cdot 10^{-6}$	Calibrated
$\hat{\epsilon}_0$	Half saturation constant in recovery rate for carriers	10^{-6}	Calibrated
	Epidemic parameters		
d	Per capita death rate in buffalo	$6.25 \cdot 10^{-5}$	Jolles et al. (2021)
K	Buffalo carrying capacity	500000	fixed
w	Waning immunity rate	0.0068	Jolles et al. (2021)
Λ	Per capita birth rate in buffalo	1/150	fixed
ρ	Probability of becoming a carrier	0.9	Jolles et al. (2021)
	Initial Conditions		
$A(0)$	Initial value of adaptive immune response in acute infectious	$2.64 \cdot 10^{-4}$	Macdonald et al. (2022)
$I_A(0)$	Initial value of innate immune response in acute infectious	2.64	Macdonald et al. (2022)
$P(0)$	Initial value of viral load in bloodstream in acute infectious	0.016	Macdonald et al. (2022)
$A_C(0)$	Initial value of adaptive immune response in carriers	$2.64 \cdot 10^{-4}$	Same as $A(0)$
$I_C(0)$	Initial value of innate immune response in carriers	2.64	Same as $I_A(0)$
$P_C(0)$	Initial value of viral load in bloodstream in carriers	0.016	Same as $P(0)$
$P_T(0)$	Initial value of pathogen load in tonsils in carriers	0.01	fixed
$C(0)$	Initial value of carrier infected buffalo	1000	fixed
$I(0)$	Initial value of acute infected buffalo	1000	fixed
$M(0)$	Initial value of buffalo with material immunity	1000	fixed
$R(0)$	Initial value of recovered buffalo	1000	fixed
$S(0)$	Initial value of susceptible buffalo	100000	fixed

Table 3: List of parameters along with their descriptions, values, and sources. *-in Macdonald et al. (2022), was fixed as being 0, but we fix θ as being the calibrated value for θ_C so that I isn't decoupled from system (1).

Variable	Description
τ	Infection age: Time-since-host-infection for acute-infected individuals
$P(\tau)$	Pathogen load in bloodstream of an acute infectious host with infection age τ
$I_A(\tau)$	Innate immune response of an acute infectious host with infection age τ
$A(\tau)$	Adaptive immune response of an acute infectious host with infection age τ
$\hat{\tau}$	Carrier age: Time since carrier-infected host became a carrier
$P_T(\hat{\tau})$	Pathogen load in the tonsils of a carrier host with carrier age $\hat{\tau}$
$P_C(\hat{\tau})$	Pathogen load in the bloodstream of a carrier host with carrier age $\hat{\tau}$
$I_C(\hat{\tau})$	Innate immune response of a carrier host with carrier age $\hat{\tau}$
$A_C(\hat{\tau})$	Adaptive immune response of the carrier host with carrier age $\hat{\tau}$
t	Chronological time or time of the epidemic
$M(t)$	The number of individuals with maternal immunity at time t
$S(t)$	The number of susceptible individuals at time t
$i(t,\tau)$	The density of acute infectious individuals with infection age τ at time t
$R(t)$	The number of recovered individuals at time t
$c(t,\tau)$	The density of the carrier individuals with carrier age τ at time t

Table 4: Description of state variables and time variables

3.1 Existence and the stability of the DFE

We derive the steady state solutions to the epidemiological model (8) by setting the derivatives with respect to t equal to zero:

$$
\begin{aligned}
0 &= \Lambda\left(R+\int_0^\infty c(\hat{\tau})\,\mathrm{d}\hat{\tau}\right)\left(1-\frac{N}{K}\right)-dM-wM,\\
0 &= \Lambda\left(S+\int_0^\infty i(\tau)\,\mathrm{d}\tau\right)\left(1-\frac{N}{K}\right)+wM-S\left(\int_0^\infty \beta(\tau)i(\tau)\,\mathrm{d}\tau+\int_0^\infty \beta_C(\hat{\tau})c(\hat{\tau})\,\mathrm{d}\hat{\tau}\right)-dS,\\
\frac{\partial i}{\partial \tau} &= -(\gamma(\tau)+d)\,i(\tau),\\
i(0) &= S\left(\int_0^\infty \beta(\tau)i(\tau)\,\mathrm{d}\tau+\int_0^\infty \beta_C(\hat{\tau})c(\hat{\tau})\,\mathrm{d}\hat{\tau}\right),\\
0 &= (1-\rho)\int_0^\infty \gamma(\tau)i(\tau)\,\mathrm{d}\tau+\int_0^\infty \alpha(\hat{\tau})c(\hat{\tau})\,\mathrm{d}\hat{\tau}-dR,\\
\frac{\partial c}{\partial \hat{\tau}} &= -(\alpha(\hat{\tau})+d)\,c(\hat{\tau}),\\
c(0) &= \rho\int_0^\infty \gamma(\tau)i(\tau)\,\mathrm{d}\tau
\end{aligned}
$$

The system (8) has a DFE

$$\mathscr{E}_0 = (0, \hat{S}_0, 0, 0, 0), \tag{12}$$

where $\hat{S}_0 = K\,(1-d/\Lambda)$.

Next, we show that $\mathcal{R}_0$ is a threshold condition for the local stability of the DFE:

Theorem 3.1. *The disease-free equilibrium $\mathscr{E}_0$ (12) is locally asymptotically stable if $\mathcal{R}_0 < 1$. Otherwise, if $\mathcal{R}_0 > 1$, it is unstable.*

Proof. We linearize the system around the DFE, $\mathscr{E}_0$, to determine conditions for stability. We consider solutions near the DFE by setting

$$M(t) = u(t), \quad S(t) = \hat{S}_0 + v(t), \quad i(\tau, t) = x(\tau, t),$$
$$R(t) = y(t), \quad c(\hat{\tau}, t) = z(\hat{\tau}, t), \text{ and } N(t) = \hat{N}_0 + n(t)$$

where $\hat{N}_0 = \hat{S}_0$. Substituting the perturbed solutions into equation (8): we obtain the following linearized system:

$$\begin{aligned}
u'(t) &= \Lambda \left(y(t) + \int_0^\infty z(\hat{\tau}, t)\, \mathrm{d}\hat{\tau} \right) \left(1 - \frac{\hat{S}_0}{K} \right) - du(t) - wu(t) \\
v'(t) &= \Lambda \left(v(t) + \int_0^\infty x(\tau, t)\, \mathrm{d}\tau \right) \left(1 - \frac{\hat{S}_0}{K} \right) + wu(t) - dv(t) \\
&\quad - \Lambda \hat{S}_0 \frac{n(t)}{K} - \hat{S}_0 \left[\int_0^\infty \beta(\tau) x(\tau, t)\, \mathrm{d}\tau + \int_0^\infty \beta_C(\hat{\tau}) z(\hat{\tau}, t)\, \mathrm{d}\hat{\tau} \right] \\
x_\tau(\tau, t) + x_t(\tau, t) &= -(\gamma(\tau) + d) x(\tau, t) \\
x(0, t) &= \hat{S}_0 \left[\int_0^\infty \beta(\tau) x(\tau, t)\, \mathrm{d}\tau + \int_0^\infty \beta_C(\hat{\tau}) z(\hat{\tau}, t)\, \mathrm{d}\hat{\tau} \right] \\
y'(t) &= (1 - \rho) \int_0^\infty \gamma(\tau) x(\tau, t)\, \mathrm{d}\tau + \int_0^\infty \alpha(\hat{\tau}) z(\hat{\tau}, t)\, \mathrm{d}\hat{\tau} - dy(t) \\
z_{\hat{\tau}}(\hat{\tau}, t) + z_t(\hat{\tau}, t) &= -(\alpha(\hat{\tau}) + d) z(\hat{\tau}, t) \\
z(0, t) &= \rho \int_0^\infty \gamma(\tau) x(\tau, t)\, \mathrm{d}\tau.
\end{aligned}$$

We then seek solutions to the above system that are of the form $u(t) = \bar{u}e^{\lambda t}$, $v(t) = \bar{v}e^{\lambda t}$, $x(\tau, t) = \bar{x}(\tau)e^{\lambda t}$, $y(t) = \bar{y}e^{\lambda t}$, $z(\hat{\tau}, t) = \bar{z}(\hat{\tau})e^{\lambda t}$, and $n(t) = \bar{n}e^{\lambda t}$ where λ is either real or complex. Substituting the time-dependent solutions with the separable

ones and canceling $e^{\lambda t}$, we obtain the following linear eigenvalue problem:

$$
\begin{aligned}
0 &= -(\lambda + d + w)\bar{u} + \Lambda \left(\bar{y} + \int_0^\infty \bar{z}(\hat{\tau})\,\mathrm{d}\hat{\tau} \right) \left(1 - \frac{\hat{S}_0}{K} \right) \\
0 &= -(\lambda + d)\bar{v} + \Lambda \left(\bar{v} + \int_0^\infty \bar{x}(\tau)\,\mathrm{d}\tau \right) \left(1 - \frac{\hat{S}_0}{K} \right) + w\bar{u} \\
&\quad - \Lambda \hat{S}_0 \frac{\bar{n}}{K} - \hat{S}_0 \left[\beta(\tau)\bar{x}(\tau)\,\mathrm{d}\tau + \int_0^\infty \beta_C(\hat{\tau})\bar{z}(\hat{\tau})\,\mathrm{d}\hat{\tau} \right] \\
\frac{\mathrm{d}\bar{x}(\tau)}{\mathrm{d}\tau} &= -(\lambda + \gamma(\tau) + d)\bar{x}(\tau) \\
\bar{x}(0) &= \hat{S}_0 \left[\int_0^\infty \beta(\tau)\bar{x}(\tau)\,\mathrm{d}\tau + \int_0^\infty \beta_C(\hat{\tau})\bar{z}(\hat{\tau})\,\mathrm{d}\hat{\tau} \right] \\
0 &= -(\lambda + d)\bar{y} + (1-\rho) \int_0^\infty \gamma(\tau)\bar{x}(\tau)\,\mathrm{d}\tau + \int_0^\infty \alpha \bar{z}(\hat{\tau})\,\mathrm{d}\hat{\tau} \\
\frac{\mathrm{d}\bar{z}(\hat{\tau})}{\mathrm{d}\hat{\tau}} &= -(\lambda + \alpha(\hat{\tau}) + d)\bar{z}(\hat{\tau}) \\
\bar{z}(0) &= \rho \int_0^\infty \gamma(\tau)\bar{x}(\tau)\,\mathrm{d}\tau.
\end{aligned}
\tag{13}
$$

From the fourth equation in (13), we obtain

$$
\bar{x}(\tau) = \bar{x}(0)e^{\lambda\tau}\pi(\tau). \tag{14}
$$

By the sixth equation in (13), we have

$$
\bar{z}(\hat{\tau}) = \bar{z}(0)e^{\lambda\hat{\tau}}\pi_C(\hat{\tau}). \tag{15}
$$

By substituting (14) into the last equation of the system (13), we get a solution for $\bar{z}(0)$ which is a function of $\bar{x}(0)$:

$$
\bar{z}(0) = \rho \int_0^\infty \bar{x}(0)\gamma(\tau)e^{-\lambda\tau}\pi(\tau)\,\mathrm{d}\tau \tag{16}
$$

By substituting (14)-(16) into the third equation in (13) and then canceling $\bar{z}(0)$, we obtain the characteristic equation $\mathscr{G}(\lambda) = 1$, where

$$
\mathscr{G}(\lambda) = \hat{S}_0 \left[\int_0^\infty \beta(\tau)e^{-\lambda\tau}\pi(\tau)\,\mathrm{d}\tau + \rho \int_0^\infty \gamma(\tau)e^{-\lambda\tau}\pi(\tau)\,\mathrm{d}\tau \int_0^\infty \beta_C(\hat{\tau})e^{-\lambda\hat{\tau}}\pi_C(\hat{\tau})\,\mathrm{d}\hat{\tau} \right]. \tag{17}
$$

Note that $\mathcal{R}_0 = \mathscr{G}(0)$, where

$$
\mathcal{R}_0 = \hat{S}_0 \left[\int_0^\infty \beta(\tau)\pi(\tau)\,\mathrm{d}\tau + \rho \int_0^\infty \gamma(\tau)\pi(\tau)\,\mathrm{d}\tau \int_0^\infty \beta_C(\hat{\tau})\pi_C(\hat{\tau})\,\mathrm{d}\hat{\tau} \right].
$$

The DFE, $\mathscr{E}_0$, that is given in (12) is locally asymptotically stable if all eigenvalues λ have negative real parts, and $\mathcal{E}_0$ is unstable if there exist a solution λ with positive real part.

Let $\lambda \in \mathbb{R}$ and consider the function $\mathscr{G}(\lambda)$ given in (17). If there is some positive interval for which $\beta(\tau)$ is strictly positive or if there is some positive function for which both $\beta_C(\hat{\tau})$ and $\gamma(\tau)$ are strictly positive, then

$$\frac{\mathrm{d}\mathscr{G}(\lambda)}{\mathrm{d}\lambda} = -\hat{S}_0 \left[\int_0^\infty \beta(\tau)\tau e^{-\lambda\tau}\pi(\tau)\,\mathrm{d}\tau + \rho \int_0^\infty \gamma(\tau)\tau e^{-\lambda\tau}\pi(\tau)\,\mathrm{d}\tau \int_0^\infty \beta_C(\hat{\tau})\hat{\tau} e^{-\lambda\hat{\tau}}\pi_C(\hat{\tau})\,\mathrm{d}\hat{\tau} \right] < 0.$$

Thus, $\mathscr{G}$ is a decreasing function of λ, and

$$\lim_{\lambda\to\infty} \mathscr{G}(\lambda) = 0.$$

When $\mathcal{R}_0 = \mathscr{G}(0) > 1$, there exists a unique positive real solution to the equation $\mathscr{G}(\lambda) = 1$ by Intermediate Value Theorem. Therefore $\mathcal{R}_0 > 1$ implies that $\mathcal{E}_0$ is unstable.

Next, we consider the case where $\mathcal{R}_0 = \mathscr{G}(0) < 1$. Let $\lambda = a + bi$ be an eigenvalue with nonnegative real part a. Then

$$\begin{aligned}
1 &= |\mathscr{G}(a+bi)| \\
&\le \hat{S}_0 \left[\int_0^\infty \beta(\tau)e^{-a\tau}\left|e^{-ib\tau}\right|\pi(\tau)\,\mathrm{d}\tau + \rho \int_0^\infty \gamma(\tau)e^{-a\tau}\left|e^{-ib\tau}\right|\pi(\tau)\,\mathrm{d}\tau \int_0^\infty \beta_C(\hat{\tau})e^{-a\hat{\tau}}\left|e^{-ib\hat{\tau}}\right|\pi_C(\hat{\tau})\,\mathrm{d}\hat{\tau} \right] \\
&= \hat{S}_0 \left[\int_0^\infty \beta(\tau)e^{-a\tau}\pi(\tau)\,\mathrm{d}\tau + \rho \int_0^\infty \gamma(\tau)e^{-a\tau}\pi(\tau)\,\mathrm{d}\tau \int_0^\infty \beta_C(\hat{\tau})e^{-a\hat{\tau}}\pi_C(\hat{\tau})\,\mathrm{d}\hat{\tau} \right] \le \mathcal{R}_0 < 1,
\end{aligned}$$

which is a contradiction. Therefore all eigenvalues have negative real parts when $\mathcal{R}_0 < 1$. This completes the proof. □

3.2 Existence of the endemic equilibrium

Next, we will show the existence of an endemic (positive) equilibrium $\mathscr{E}^* = (M^*, S^*, i^*(\tau), R^*, c^*(\tau))$ of the system (8) when $\mathcal{R}_0 > 1$.

First, we establish the following result:

Lemma 3.2. *Let* $\Pi = \int_0^\infty \pi(\tau)\,\mathrm{d}\tau$, *and* $\Pi_C = \int_0^\infty \pi_C(\hat{\tau})\,\mathrm{d}\hat{\tau}$ *(where* $\pi(\tau) = e^{-\int_0^\tau (\gamma(s)+d)\,\mathrm{d}s}$ *and* $\pi_C(\hat{\tau}) = e^{-\int_0^{\hat{\tau}} (\alpha(s)+d)\,\mathrm{d}s}$*). Define*

$$\Gamma = \left(1 - \rho + \rho \int_0^\infty \alpha(\hat{\tau})\pi_C(\hat{\tau})\,\mathrm{d}\hat{\tau}\right) \int_0^\infty \gamma(\tau)\pi(\tau)\,\mathrm{d}\tau, \tag{18a}$$

$$\chi = \frac{\Gamma}{d} + \rho\Pi_C \int_0^\infty \gamma(\tau)\pi(\tau)\,\mathrm{d}\tau, \text{ and} \tag{18b}$$

$$\mathcal{Y} = \chi + \Pi. \tag{18c}$$

We can further simplify χ *and* $\mathcal{Y}$ *as follows:*

$$\chi = \frac{1}{d} \int_0^\infty \gamma(\tau)\pi(\tau)\,\mathrm{d}\tau \tag{19a}$$

$$\mathcal{Y} = \frac{1}{d}. \tag{19b}$$

Proof. Observe $\frac{\mathrm{d}}{\mathrm{d}\hat{\tau}}\pi_C(\hat{\tau}) = -(\alpha(\hat{\tau})+d)\pi_C(\hat{\tau})$ and $\frac{\mathrm{d}}{\mathrm{d}\tau}\pi(\tau) = -(\gamma(\tau)+d)\pi(\tau)$. We can use these derivatives to simplify χ and $\mathcal{Y}$ (Note: for simplifying χ we also use (18a)).

$$\begin{aligned}
\chi &= \frac{\Gamma}{d} + \rho\Pi_C \int_0^\infty \gamma(\tau)\pi(\tau)\,\mathrm{d}\tau \\
&= \frac{1}{d}\left(1-\rho+\rho\int_0^\infty (\alpha(\hat{\tau})+d)\pi_C(\hat{\tau})\,\mathrm{d}\hat{\tau}\right)\int_0^\infty \gamma(\tau)\pi(\tau)\,\mathrm{d}\tau \\
&= \frac{1}{d}\left(1-\rho+\rho\left[-\pi_C(\hat{\tau})|_0^\infty\right]\right)\int_0^\infty \gamma(\tau)\pi(\tau)\,\mathrm{d}\tau \\
&= \frac{1}{d}\int_0^\infty \gamma(\tau)\pi(\tau)\,\mathrm{d}\tau,
\end{aligned}
\qquad
\begin{aligned}
\mathcal{Y} &= \chi + \Pi \\
&= \frac{1}{d}\int_0^\infty \gamma(\tau)\pi(\tau)\,\mathrm{d}\tau + \int_0^\infty \pi(\tau)\,\mathrm{d}\tau \\
&= \frac{1}{d}\left[\int_0^\infty (\gamma(\tau)+d)\pi(\tau)\,\mathrm{d}\tau\right] \\
&= \frac{1}{d}.
\end{aligned}$$

□

Theorem 3.3. *If $\mathcal{R}_0 > 1$, then there exists a unique endemic equilibrium, $\mathscr{E}$, to system (8) with its components being the following:*

$$M^* = \frac{i^*(0)\Lambda\chi\left(K - \frac{\hat{S}_0}{\mathcal{R}_0} - i^*(0)\mathcal{Y}\right)}{i^*(0)\Lambda\chi + K(d+w)} \tag{20a}$$

$$S^* = \frac{\hat{S}_0}{\mathcal{R}_0} \tag{20b}$$

$$i^*(\tau) = i^*(0)\pi(\tau) \tag{20c}$$

$$R^* = \frac{\Gamma}{d} i^*(0) \tag{20d}$$

$$c^*(\hat{\tau}) = i^*(0)\rho\left(\int_0^\infty \gamma(\tau)\pi(\tau)\,\mathrm{d}\tau\right)\pi_C(\hat{\tau}) \tag{20e}$$

where Γ, χ, and $\mathcal{Y}$ are the numbers defined in Lemma 3.2.

For the components M^*, $i^*(\tau)$, R^*, and $c^*(\hat{\tau})$, the component $i^*(0)$ must be the root of the following quadratic polynomial

$$g(i(0)) = A_2(i(0))^2 + A_1 i(0) + A_0 \tag{21}$$

with coefficients

$$A_2 = -\mathcal{R}_0[(d\Pi + w\mathcal{Y})\mathcal{Y} + \chi] \tag{22}$$

$$A_1 = (K\mathcal{R}_0 - \hat{S}_0)(d\Pi + w\mathcal{Y}) - (d+w)\left(\frac{K\mathcal{R}_0}{\Lambda} + \mathcal{Y}\hat{S}_0\right) - \chi d\hat{S}_0 \tag{23}$$

$$A_0 = (d+w)\hat{S}_0^2\left[1 - \frac{1}{\mathcal{R}_0}\right]. \tag{24}$$

Proof. The equilibria of the epidemiological model are obtained by setting the time t derivatives of the model to zero:

$$0 = \Lambda\left(R + \int_0^\infty c(\hat{\tau})\,\mathrm{d}\hat{\tau}\right)\left(1 - \frac{N}{K}\right) - dM - wM, \tag{25}$$

$$0 = \Lambda \left(S + \int_0^\infty i(\tau)\,\mathrm{d}\tau \right) \left(1 - \frac{N}{K} \right) + wM - S \left(\int_0^\infty \beta(\tau) i(\tau)\,\mathrm{d}\tau + \int_0^\infty \beta_C(\hat{\tau}) c(\hat{\tau})\,\mathrm{d}\hat{\tau} \right) - dS, \tag{26}$$

$$\frac{\partial i}{\partial \tau} = -(\gamma(\tau) + d)\; i(\tau), \tag{27}$$

$$i(0) = S \left(\int_0^\infty \beta(\tau) i(\tau)\,\mathrm{d}\tau + \int_0^\infty \beta_C(\hat{\tau}) c(\hat{\tau})\,\mathrm{d}\hat{\tau} \right), \tag{28}$$

$$0 = (1-\rho) \int_0^\infty \gamma(\tau) i(\tau)\,\mathrm{d}\tau + \int_0^\infty \alpha(\hat{\tau}) c(\hat{\tau})\,\mathrm{d}\hat{\tau} - dR, \tag{29}$$

$$\frac{\partial c}{\partial \hat{\tau}} = -(\alpha(\hat{\tau}) + d)\; c(\hat{\tau}), \tag{30}$$

$$c(0) = \rho \int_0^\infty \gamma(\tau) i(\tau)\,\mathrm{d}\tau. \tag{31}$$

By first solving the differential equation (27), we obtain:

$$i^*(\tau) = i^*(0)\pi(\tau). \tag{32}$$

Similarly, we solve the differential equation (30)

$$c^*(\hat{\tau}) = c^*(0)\pi_C(\hat{\tau}). \tag{33}$$

Then substituting (32) into equation (31), we get

$$c^*(0) = \rho \int_0^\infty \gamma(\tau) i^*(0) \pi(\tau)\,\mathrm{d}\tau. \tag{34}$$

Substituting the expressions for $i^*(\tau)$, $c^*(\hat{\tau})$, and $c^*(0)$ into equation (28) and canceling the $i^*(0)$ yields the expression below:

$$1 = S^* \left[\int_0^\infty \beta(\tau)\pi(\tau)\,\mathrm{d}\tau + \rho \int_0^\infty \gamma(\tau)\pi(\tau) d\tau \int_0^\infty \beta_C(\hat{\tau})\pi_C(\hat{\tau})\,\mathrm{d}\tau \right].$$

We rearrange terms in the above equation and use (10) to obtain the following:

$$S^* = \frac{\hat{S}_0}{\mathcal{R}_0}. \tag{35}$$

From equation (29), we have

$$R^* = \frac{i^*(0)}{d} \left[\left(1 - \rho + \rho \int_0^\infty \alpha(\hat{\tau})\pi_C(\hat{\tau})\,\mathrm{d}\hat{\tau} \right) \int_0^\infty \gamma(\tau)\pi(\tau)\,\mathrm{d}\tau \right].$$

Now, we substitute the expression of Γ given in (18a) to rewrite R^* as follows:

$$R^* = \frac{\Gamma}{d} i^*(0). \tag{36}$$

Note that in solving the equation (25), we obtain

$$M^* = \frac{\Lambda\left(R^* + \int_0^\infty c^*(\hat{\tau})\,\mathrm{d}\hat{\tau}\right)\left(K - S^* - \int_0^\infty i^*(\tau)\,\mathrm{d}\tau - R^* - \int_0^\infty c^*(\hat{\tau})\,\mathrm{d}\hat{\tau}\right)}{\Lambda\left(R^* + \int_0^\infty c^*(\hat{\tau})\,\mathrm{d}\hat{\tau}\right) + K(d+w)}.$$

Also note that

$$R^* + \int_0^\infty c^*(\hat{\tau})\,\mathrm{d}\hat{\tau} = \left(\frac{\Gamma}{d} + \rho\int_0^\infty \pi_C(\hat{\tau})\,\mathrm{d}\hat{\tau}\int_0^\infty \gamma(\tau)\pi(\tau)\,\mathrm{d}\tau\right) i^*(0) = \chi i^*(0),$$

where χ is given in (18b). Using equations (32), (35), (18c), and the above equality, we re-express M^* in terms of $i^*(0)$

$$M^* = \frac{i^*(0)\Lambda\chi\left(K - \frac{\hat{S}_0}{\mathcal{R}_0} - (\Pi+\chi)i^*(0)\right)}{i^*(0)\Lambda\chi + K(d+w)} = \frac{i^*(0)\Lambda\chi\left(K - \frac{\hat{S}_0}{\mathcal{R}_0} - i^*(0)\mathcal{Y}\right)}{i^*(0)\Lambda\chi + K(d+w)}. \tag{37}$$

Now, we utilize equation (26) to find $i^*(0)$. First, we use (28) to rewrite equation (26) as

$$0 = \Lambda\left(S^* + \int_0^\infty i^*(\tau)\,\mathrm{d}\tau\right)\left(1 - \frac{N^*}{K}\right) + wM^* - i^*(0) - dS^*.$$

Observe that

$$i^*(0)\mathcal{Y} = \int_0^\infty i^*(\tau)\,\mathrm{d}\tau + R^* + \int_0^\infty c^*(\hat{\tau})\,\mathrm{d}\hat{\tau}.$$

Thus, $N^* = S^* + i^*(0)\mathcal{Y} + M^*$. Multiplying both sides of the above equation by K and re-expressing N^* yields

$$0 = \Lambda\left(S^* + \int_0^\infty i^*(\tau)\,\mathrm{d}\tau\right)(K - S^* - i^*(0)\mathcal{Y} - M^*) + KwM^* - Ki^*(0) - KdS^*.$$

We substitute expressions for S^*, M^*, and $i^*(\tau)$ into the above equation to obtain the following:

$$\begin{aligned} 0 = \Lambda\left(\frac{\hat{S}_0}{\mathcal{R}_0} + i^*(0)\Pi\right)&\left(K - \frac{\hat{S}_0}{\mathcal{R}_0} - i^*(0)\mathcal{Y} - \frac{i^*(0)\Lambda\chi\left(K - \frac{\hat{S}_0}{\mathcal{R}_0} - i^*(0)\mathcal{Y}\right)}{i^*(0)\Lambda\chi + K(d+w)}\right) \\ &+ \frac{Kwi^*(0)\Lambda\chi\left(K - \frac{\hat{S}_0}{\mathcal{R}_0} - i^*(0)\mathcal{Y}\right)}{i^*(0)\Lambda\chi + K(d+w)} - K(i^*(0)) - Kd\frac{\hat{S}_0}{\mathcal{R}_0}. \end{aligned}$$

Multiplying both sides of the above equation by $i^*(0)\Lambda\chi + K(d+w)$ and $\mathcal{R}_0$ and dividing both sides by K yields:

$$\begin{aligned} 0 =& \Lambda\left[K\mathcal{R}_0 - \hat{S}_0 - \mathcal{R}_0\mathcal{Y}i^*(0)\right]\left[(d+w)\left(\frac{\hat{S}_0}{\mathcal{R}_0} + \Pi i^*(0)\right) + w\chi i^*(0)\right] \\ &- \left(\mathcal{R}_0 i^*(0) + d\hat{S}_0\right)\left(\Lambda\chi i^*(0) + K(d+w)\right). \end{aligned}$$

Distributing terms and using $\mathcal{Y} = \chi + \Pi$ yields

$$\begin{aligned}
0 = &-\mathcal{R}_0\Lambda[(d\Pi + w\mathcal{Y})\mathcal{Y} + \chi](i^*(0))^2 \\
&+ [\Lambda(K\mathcal{R}_0 - \hat{S}_0)(d\Pi + w\mathcal{Y}) - (d+w)[K\mathcal{R}_0 + \Lambda\mathcal{Y}\hat{S}_0] - \Lambda\chi d\hat{S}_0]i^*(0) \\
&+ (d+w)\hat{S}_0\left[K(\Lambda - d) - \Lambda\frac{\hat{S}_0}{\mathcal{R}_0}\right].
\end{aligned}$$

We rewrite the constant term in the above equation by using $\hat{S}_0 = K(\Lambda - d)/\Lambda$ and divide both sides of the above equation by Λ to obtain

$$g(i(0)) = A_2(i(0))^2 + A_1 i(0) + A_0 = 0$$

with coefficients

$$\begin{aligned}
A_2 &= -\mathcal{R}_0[(d\Pi + w\mathcal{Y})\mathcal{Y} + \chi], \\
A_1 &= (K\mathcal{R}_0 - \hat{S}_0)(d\Pi + w\mathcal{Y}) - (d+w)\left(\frac{K\mathcal{R}_0}{\Lambda} + \mathcal{Y}\hat{S}_0\right) - \chi d\hat{S}_0, \\
A_0 &= (d+w)\hat{S}_0^2\left[1 - \frac{1}{\mathcal{R}_0}\right],
\end{aligned}$$

which are the coefficients (22)-(24) of the polynomial (21). Notice that the sign of A_2 is always negative and that the sign of A_0 is positive whenever $\mathcal{R}_0 > 1$. Then, by Descartes' Rule of Signs, $\mathcal{R}_0 > 1$ implies that polynomial $g(i(0))$ has exactly one positive root, which is of the form

$$i^*(0) = \frac{A_1 + \sqrt{A_1^2 - 4A_0A_2}}{2|A_2|}.$$

Lastly, we show that the unique positive root satisfies

$$i^*(0) < \frac{1}{\mathcal{Y}}\left(K - \frac{\hat{S}_0}{\mathcal{R}_0}\right), \tag{38}$$

which ensures that M^* is positive. Observe when $\mathcal{R}_0 > 1$, the quadratic polynomial g is a parabola that opens down with the y-intercept lying above the x-axis. Therefore for verifying inequality (38), it suffices to show that

$$g\left(\frac{1}{\mathcal{Y}}\left[K - \frac{\hat{S}_0}{\mathcal{R}_0}\right]\right) < 0$$

when $\mathcal{R}_0 > 1$. We evaluate g at $(1/\mathcal{Y})[K - \hat{S}_0/\mathcal{R}_0]$, simplify, and rearrange terms to obtain

$$g\left(\frac{K - \frac{\hat{S}_0}{\mathcal{R}_0}}{\mathcal{Y}}\right) = -\frac{\mathcal{R}_0\chi\left(K - \frac{\hat{S}_0}{\mathcal{R}_0}\right)^2}{\mathcal{Y}^2} - \frac{(d+w)}{\mathcal{Y}}\left(\frac{K\mathcal{R}_0}{\Lambda} + \mathcal{Y}\hat{S}_0\right)\left(K - \frac{\hat{S}_0}{\mathcal{R}_0}\right) - \frac{\chi d\hat{S}_0}{\mathcal{Y}}\left(K - \frac{\hat{S}_0}{\mathcal{R}_0}\right) + A_0. \tag{39}$$

Note that the term $(K - \hat{S}_0/\mathcal{R}_0) > 0$ since $\hat{S}_0 < K$ and $1/\mathcal{R}_0 < 1$ when $\mathcal{R}_0 > 1$. All terms of the right-hand side of the above equality are negative except the last term, A_0. We combine the second term with the last term (but replace A_0 with (24)) of the right-hand side of (39) with the last term (substituting to form the following expression:

$$W = -\frac{(d+w)}{\mathcal{Y}}\left(\frac{K\mathcal{R}_0}{\Lambda} + \mathcal{Y}\hat{S}_0\right)\left(K - \frac{\hat{S}_0}{\mathcal{R}_0}\right) + (d+w)\hat{S}_0^2\left(1 - \frac{1}{\mathcal{R}_0}\right).$$

We show that the sign of W is negative to verify that the right-side of (39) is negative. We use $\hat{S}_0 = K(1 - d/\Lambda)$ to simplify the expression W to get

$$\begin{aligned} W &= -\frac{(d+w)}{\mathcal{Y}}\left(\frac{K}{\Lambda}(\mathcal{R}_0 - 1) + \mathcal{Y}K\right)\left(K - \frac{\hat{S}_0}{\mathcal{R}_0}\right) + (d+w)\hat{S}_0 K\left(1 - \frac{d}{\Lambda}\right)\left(1 - \frac{1}{\mathcal{R}_0}\right) \\ &= -(d+w)K\left[\frac{(\mathcal{R}_0 - 1)}{\mathcal{Y}\Lambda}\left(K - \frac{\hat{S}_0}{\mathcal{R}_0}\right) + \left(K - \frac{\hat{S}_0}{\mathcal{R}_0}\right) - \hat{S}_0\left(1 - \frac{1}{\mathcal{R}_0}\right) + \frac{\hat{S}_0}{\mathcal{R}_0}\left(\frac{d}{\Lambda}\right)\right] \\ &= -\frac{(d+w)K}{\mathcal{Y}\Lambda}(\mathcal{R}_0 - 1)\left(K - \frac{\hat{S}_0}{\mathcal{R}_0}\right) - (d+w)K(K - \hat{S}_0) - (d+w)\hat{S}_0 K\left(\frac{d}{\Lambda}\right)\frac{1}{\mathcal{R}_0} < 0. \end{aligned}$$

This completes our proof. □

The presence of the quadratic equation (21) causes one to consider the plausibility of backward bifurcation. In our case, we have shown uniqueness of an endemic equilibrium when $\mathcal{R}_0 > 1$. However, the system may have up to two interior endemic equilibria when $\mathcal{R}_0 < 1$, in which case the system may display backward bifurcation (Barfield et al., 2018; Gulbudak et al., 2021; Gulbudak and Martcheva, 2013; Welker and Marcheva, 2020). Thus, we explore the bifurcation dynamics of the system and show that it can present forward bifurcation for some epidemiological parameters. To investigate bifurcation, we consider three parameters, $p \in \{\rho, K, \Lambda\}$, that appear explicitly in $\mathcal{R}_0$. We view p as being a potential bifurcation parameter. In order to investigate how the dynamics change with respect to changes in p, we consider thresholds as functions of p and solve $\mathcal{R}_0(p) = 1$ and denote the critical value as being p_{crit}. In particular, we have

$$\mathcal{R}_0(\rho_{\text{crit}}) = 1 \iff \rho_{\text{crit}} = \frac{1 - \hat{S}_0\int_0^\infty \beta(\tau)\pi(\tau)\,\mathrm{d}\tau}{\hat{S}_0\int_0^\infty \gamma(\tau)\pi(\tau)\,\mathrm{d}\tau\int_0^\infty \beta_C(\hat{\tau})\pi_C(\hat{\tau})\,\mathrm{d}\hat{\tau}},$$

$$\mathcal{R}_0(K_{\text{crit}}) = 1 \iff K_{\text{crit}} = \frac{1}{\left(1 - \frac{d}{\Lambda}\right)\left[\int_0^\infty \beta(\tau)\pi(\tau)\,\mathrm{d}\tau + \rho\int_0^\infty \gamma(\tau)\pi(\tau)\,\mathrm{d}\tau\int_0^\infty \beta_C(\hat{\tau})\pi_C(\hat{\tau})\,\mathrm{d}\hat{\tau}\right]},$$

and

$$\mathcal{R}_0(\Lambda_{\text{crit}}) = 1 \iff \Lambda_{\text{crit}} = \frac{dK}{K - \frac{1}{\int_0^\infty \beta(\tau)\pi(\tau)\,\mathrm{d}\tau + \rho\int_0^\infty \gamma(\tau)\pi(\tau)\,\mathrm{d}\tau \int_0^\infty \beta_C(\hat{\tau})\pi_C(\hat{\tau})\,\mathrm{d}\hat{\tau}}}.$$

In the latter case, the value of Λ_{crit} is positive since the number $K[\int_0^\infty \beta(\tau)\pi(\tau)\,\mathrm{d}\tau + \rho\int_0^\infty \gamma(\tau)\pi(\tau)\,\mathrm{d}\tau \int_0^\infty \beta_C(\hat{\tau})\pi_C(\hat{\tau})\,\mathrm{d}\hat{\tau}] > 1$.

We use the Implicit Function Theorem to show that only forward bifurcation occurs for these parameters at the critical parameter values.

Theorem 3.4. *The system (8) has forward bifurcation at $p = p_{crit}$, $I^* = 0$ (where p_{crit} is the critical parameter value that gives $\mathcal{R}_0(p_{crit}) = 1$ and $p \in \{\rho, K, \Lambda\}$).*

Proof. Let p be our bifurcation parameter and let p_{crit} our critical value for which $\mathcal{R}_0(p_{\text{crit}}) = 1$. Now let $I^* = \int_0^\infty i^*(0)\pi(\tau)\,\mathrm{d}\tau$. We look at the sign of

$$\left.\frac{\partial I^*}{\partial p}\right|_{(p=p_{\text{crit}}, I^*=0)}.$$

The system has backward bifurcation at $p = p_{\text{crit}}$ if and only if

$$\left.\frac{\partial I^*}{\partial p}\right|_{(p=p_{\text{crit}}, I^*=0)} < 0,$$

and the system has forward bifurcation at $p = p_{\text{crit}}$ if and only if

$$\left.\frac{\partial I*}{\partial p}\right|_{(p=p_{\text{crit}}, I^*=0)} > 0.$$

Notice that

$$\text{sign}\left(\left.\frac{\partial i^*(0)}{\partial p}\right|_{(p=p_{\text{crit}}, i^*(0)=0)}\right) = \text{sign}\left(\left.\frac{\partial I^*}{\partial p}\right|_{(p=p_{\text{crit}}, I^*=0)}\right).$$

In our bifurcation analysis, we investigate the sign of the

$$\left.\frac{\partial i^*(0)}{\partial p}\right|_{(p=p_{\text{crit}}, i^*(0)=0)}.$$

By differentiating the polynomial equation (21) implicitly with respect to parameter p, evaluating at $p = p_{\text{crit}}$ and $i^*(0) = 0$, and solving for $\partial i^*(0)/\partial p$ (at $p = p_{\text{crit}}$ and $i^*(0) = 0$), we obtain

$$\left.\frac{\partial i^*(0)}{\partial p}\right|_{(p=p_{\text{crit}}, i^*(0)=0)} = \frac{-\left.\frac{\partial A_0}{\partial p}\right|_{(p=p_{\text{crit}}, i^*(0)=0)}}{A_1(p_{\text{crit}})}. \tag{40}$$

We now show that the right hand side of the above equality is positive for each parameter being investigated.

Case 1 ($p = \rho$): First we compute the partial of coefficient A_0 with respect to ρ:

$$\frac{\partial A_0}{\partial \rho} = (d+w)\hat{S}_0 \frac{1}{\mathcal{R}_0^2} \frac{\partial \mathcal{R}_0}{\partial \rho}$$

where

$$\frac{\partial \mathcal{R}_0}{\partial \rho} = \hat{S}_0 \int_0^\infty \gamma(\tau)\pi(\tau)d\tau \int_0^\infty \beta_C(\hat{\tau})\pi_C(\hat{\tau})d\hat{\tau} > 0.$$

We then have

$$-\frac{\partial A_0}{\partial \rho}\bigg|_{(p=p_{\text{crit}}, i^*(0)=0)} = (d+w)\hat{S}_0 \frac{\partial \mathcal{R}_0}{\partial \rho} < 0.$$

We now determine the sign of $A_1(\rho_{\text{crit}})$ (note through simplifications obtained on the numbers χ and $\mathcal{Y}$, coefficient A_1's dependence on parameter ρ is only through $\mathcal{R}_0$). We have

$$A_1(\rho_{\text{crit}}) = A_1\bigg|_{\mathcal{R}_0=1} = (K - \hat{S}_0)(d\Pi + w\mathcal{Y}) - (d+w)\left(\frac{K}{\Lambda} + \mathcal{Y}\hat{S}_0\right) - d\chi\hat{S}_0,$$

where $\hat{S}_0 = K(1 - \Lambda/d)$. In replacing $\hat{S}_0$ with $K(1 - \Lambda/d)$, we see that we can factor our K, so we analyze the sign of $A_1(\rho_{\text{crit}})/K$ to determine the sign of $A_1(\rho_{\text{crit}})$:

$$\frac{A_1(\rho_{\text{crit}})}{K} = \frac{d}{\Lambda}(d\Pi + w\mathcal{Y}) - (d+w)\left(\frac{1}{\Lambda} + \mathcal{Y}\left(1 - \frac{d}{\Lambda}\right)\right) - d\chi\left(1 - \frac{d}{\Lambda}\right).$$

Additionally, we use Lemma 3.2 (specifically, we use $\mathcal{Y} = 1/d$) to rewrite the above equation as follows:

$$\frac{A_1(\rho_{\text{crit}})}{K} = \frac{d^2}{\Lambda}\Pi + \frac{w}{\Lambda} - 1 - \frac{w}{d} - d\chi + \frac{d^2}{\Lambda}\chi.$$

Since $\mathcal{Y} = \Pi + \chi = 1/d$, the first and last terms of the right-hand side of the above equation can be combined and re-expressed as d/Λ. We apply this simplification and rearrange terms to obtain

$$\frac{A_1(\rho_{\text{crit}})}{K} = \left(1 + \frac{w}{d}\right)\left(\frac{d}{\Lambda} - 1\right) - d\chi = -\left(1 + \frac{w}{d}\right)\frac{\hat{S}_0}{K} - d\chi < 0.$$

Thus we have

$$\frac{\partial i^*(0)}{\partial p}\bigg|_{(\rho=\rho_{\text{crit}}, i^*(0)=0)} = \frac{-\frac{\partial A_0}{\partial p}\Big|_{(\rho=\rho_{\text{crit}}, i^*(0)=0)}}{A_1(p_{\text{crit}})} > 0 \tag{41}$$

when $p = \rho$.
Case 2 ($p = K$): First we compute the partial of coefficient A_0 with respect to K and evaluate at the critical parameter value:

$$\left.\frac{\partial A_0}{\partial K}\right|_{(K=K_{\text{crit}}, i^*(0)=0)} = (d+w)\left[K_{\text{crit}}\left(1-\frac{d}{\Lambda}\right)\right]^2 \frac{\partial \mathcal{R}_0}{\partial K}$$

where

$$\left.\frac{\partial \mathcal{R}_0}{K}\right|_{K=K_{\text{crit}}} = \left(1-\frac{d}{\Lambda}\right)\left[\int_0^\infty \beta(\tau)\pi(\tau)d\tau + \rho\int_0^\infty \gamma(\tau)\pi(\tau)d\tau \int_0^\infty \beta_C(\hat{\tau})\pi_C(\hat{\tau})d\hat{\tau}\right] > 0.$$

So

$$\left(1-\frac{d}{\Lambda}\right)\left[\int_0^\infty \beta(\tau)\pi(\tau)d\tau + \rho\int_0^\infty \gamma(\tau)\pi(\tau)d\tau \int_0^\infty \beta_C(\hat{\tau})\pi_C(\hat{\tau})d\hat{\tau}\right] > 0.$$

We determine the sign of $A_1(K_{\text{crit}})$ by observing

$$A_1(K_{\text{crit}}) = K_{\text{crit}}\left(\frac{d}{\Lambda}(d\Pi + w\mathcal{Y}) - (d+w)\left(\frac{1}{\Lambda} + \mathcal{Y}\left(1-\frac{d}{\Lambda}\right)\right) - d\chi\left(1-\frac{d}{\Lambda}\right)\right).$$

In Case 1, we already showed that

$$\left(\frac{d}{\Lambda}(d\Pi + w\mathcal{Y}) - (d+w)\left(\frac{1}{\Lambda} + \mathcal{Y}\left(1-\frac{d}{\Lambda}\right)\right) - d\chi\left(1-\frac{d}{\Lambda}\right)\right) - \left(1+\frac{w}{d}\right)\frac{\hat{S}_0}{K} - d\chi < 0.$$

Thus we have

$$\left.\frac{\partial i^*(0)}{\partial p}\right|_{(p=p_{\text{crit}}, i^*(0)=0)} = \frac{-\left.\frac{\partial A_0}{\partial p}\right|_{(p=p_{\text{crit}}, i^*(0)=0)}}{A_1(p_{\text{crit}})} > 0$$

when $p = K$.
Case 3 ($p = \Lambda$): First we compute the partial of coefficient A_0 with respect to Λ and evaluate at the critical parameter value:

$$\left.\frac{\partial A_0}{\partial \Lambda}\right|_{(\Lambda=\Lambda_{\text{crit}}, i^*(0)=0)} = (d+w)\left[K\left(1-\frac{d}{\Lambda_{\text{crit}}}\right)\right]^2 \frac{\partial \mathcal{R}_0}{\partial \Lambda}$$

where

$$\left.\frac{\partial \mathcal{R}_0}{\partial \Lambda}\right|_{\Lambda=\Lambda_{\text{crit}}} = \frac{Kd}{\Lambda_{\text{crit}}^2}\left[\int_0^\infty \beta(\tau)\pi(\tau)d\tau + \rho\int_0^\infty \gamma(\tau)\pi(\tau)d\tau \int_0^\infty \beta_C(\hat{\tau})\pi_C(\hat{\tau})d\hat{\tau}\right] > 0.$$

This implies that

$$\left.\frac{\partial A_0}{\partial \Lambda}\right|_{(\Lambda=\Lambda_{\text{crit}}, i^*(0)=0)} > 0.$$

We determine that the $A_1(\Lambda_{\text{crit}})$ is negative by observing

$$\text{sign}(A_1(\Lambda_{\text{crit}})) = \text{sign}\left(\frac{A_1(\Lambda_{\text{crit}})}{K}\right).$$

Through using simplifications that were used in Case 1, we obtain

$$\frac{A_1(\Lambda_{\text{crit}})}{K} = -\left(1+\frac{w}{d}\right)\left(1-\frac{d}{\Lambda_{\text{crit}}}\right) - d\chi < 0.$$

Thus we have

$$\left.\frac{\partial i^*(0)}{\partial p}\right|_{(p=p_{\text{crit}}, i^*(0)=0)} = \frac{-\left.\frac{\partial A_0}{\partial p}\right|_{(p=p_{\text{crit}}, i^*(0)=0)}}{A_1(p_{\text{crit}})} > 0$$

when $p = \Lambda$. This completes our proof. □

Notice that bifurcation analysis with respect to the within-host parameters can only be done numerically since the epidemic parameters, including β, β_C, γ, and α are formulated as functions of within-host variables, where solutions for these immunological variables can not be obtained explicitly. Furthermore due to multiple logistic terms in the system (8), analysis on the stability of the endemic equilibrium is not feasible (Tuncer et al., 2016).

4 Simulations of the immuno-epidemiological model

We develop a finite difference scheme combined with an ODE solver in MATLAB in order to numerically solve the immuno-epidemiological model. We consider the within-host model of an infectious individual during the acute phase (1) with time-since-infection ranging from $0 \leq \tau \leq \tau_{end}$. The mesh chosen for the interval $[0, \tau_{end}]$ can have equal step size $\Delta\tau$ with L mesh-points. The output of the ODE solver is the solution vector, denoted here $(\phi(\tau_j))_{j=1}^{L}$. We utilize MATLAB solver ode45, which adaptively chooses the time partition and interpolates at time points $(\tau_j)_{j=1}^{L}$. Similarly, we consider the within-host model of a carrier infected individual (2) with time since becoming a carrier ranging from $0 \leq \hat{\tau} \leq \hat{\tau}_{end}$. The mesh chosen for the interval $[0, \hat{\tau}_{end}]$ can have equal step size $\Delta\hat{\tau}$ with $\hat{L}$ mesh-points. The output of the ODE solver is the solution vector, denoted here as $(\phi(\hat{\tau}_\ell))_{\ell=1}^{\hat{L}}$. For this model, we also utilize MATLAB's solver ode45.

Moreover, in Table 3, the initial conditions for state variables A_C, I_C and P_C are set to match the initial conditions for state variables A, I_A, P. That is, the solution of the

within-carrier model would have a region for which the viral load in the bloodstream $P_C(\tau)$ is positive. On the interval $[0, \hat{\tau}_{end}]$, we find the time τ_* for which $P_C(\tau_*) < 10^{-4}$, and we assume that τ_* is the start time of the carrier phase since this is the time at which the pathogen clears in the bloodstream. In our between-host simulations, we ignore time interval $[0, \tau_*)$. Note that we can set $\tau_{end} = \tau_*$, since this can represent the duration of the acute phase.

After obtaining solution vectors for system (1) and (2), we can then discretize the linking functions. For this model we have linking functions corresponding to infected individuals during the acute stage, $f(\tau) \in \{\beta(\tau), \gamma(\tau)\}$, and corresponding to infectious individuals during the carrier stage $\hat{f}(\hat{\tau}) \in \{\beta_C(\hat{\tau}), \alpha(\hat{\tau})\}$. We can then generate a vector solution for each linking function corresponding to the acute infected, $f_j = f(\tau_j)$, (with $j = 1, \ldots, L$) and corresponding to the carrier infected $\hat{f}_\ell = \hat{f}(\hat{\tau}_\ell)$ (with $\ell = 1, \ldots, \hat{L}$). It is worth mentioning that for the simulations presented in Figure 6, linking functions $\beta_C(\hat{\tau})$ and $\alpha(\hat{\tau})$ are set to being 0 for all $\hat{\tau} < \tau_*$ since the individuals are still in acute phase.

For the epidemiological model, we approximate solutions to the age-structured PDE model with the stored within-host calculations by using a mixed implicit-explicit scheme. The numerical scheme is detailed in the Appendix Section B.

4.1 Parameter estimation

The parameter values used in the nested multi-scale model (1,2,8) are give in Table 3. The within-acute model (1) parameters came directly from our prior work Macdonald et al. (2022). The least squares approach was used to fit the model to time-series data consisting multiple needle-infected hosts during the acute stage of the disease (Perez-Martin et al., 2022). Monte Carlo simulations were also administered to assess identifiability and confidence in our fitting procedure. Some of these host may or may not have experienced a carrier stage of the disease (and such categorization was not taken into consideration during parameterization). We used the average fitted values that corresponded to the buffalo who were needle-infected with the SAT1 strain. The fitted values here represent the average immune and viral kinetics dynamics of FMD infected buffalo during the acute phase. We fixed the same values for the within-carrier model (2) but calibrate parameter values K_T, δ, η, ν, and θ_C. We calibrated these parameters by using Mathematics's manipulate feature to get a numerical solution of the ODE system whose values aligned with the mean data values of four SAT1 needle-infected buffalo during the carrier stage (note these buffalo were hosts that were studied in the data that was used in Perez-Martin et al. (2022)). To prevent the innate immune response from being decoupled from the within-acute model, we fix θ as being the calibrated value that we obtained for θ_C.

For calibrating the linking function parameters, parameter values are chosen to align with various quantities presented in Jolles et al. (2021). They estimated the infectious period for an acute phase as being 5.7 days and that the duration of the carrier phase as being 243 days. It is worth noting that the duration of the carrier stage can be longer; it can even last for years (Stenfeldt C, 2020). In Jolles et al. (2021), they approximate the basic reproduction number in the absence of carriers as being 15.8 and the basic reproduction number with carriers as being 23.8. Additionally, they

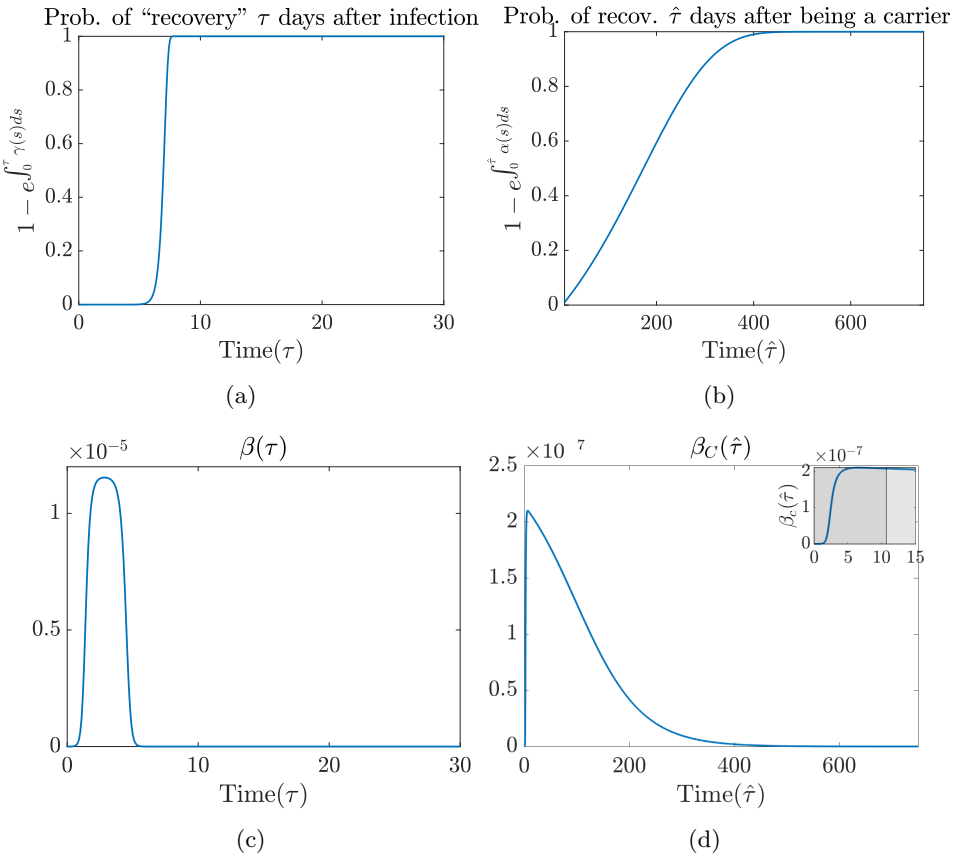

Fig. 5: **Top left.** Subfigure displays the probability of pathogen clearance in the bloodstream. **Top right.** Subfigure displays the probability of pathogen clearance in the tonsils by day $\hat{\tau}$ (after becoming a carrier). **Bottom left.** Subfigure displays the transmission rate $\beta(\tau)$ due to interacting with an acute infected individual. **Bottom right.** Subfigure displays the transmission rate $\beta_C(\hat{\tau})$ due to interacting with a carrier over time interval $[0, 750]$. The shaded inset figure shown in subfigure(d) illustrates that the start of the carrier phase $\tau_* = 10.7$. In our simulations for the nested multi-scale model, we ignore the within-host carrier dynamics on interval $[0, \tau_*)$, by setting $\beta_C(\hat{\tau}), \alpha(\hat{\tau}) = 0$ for all $\hat{\tau} < \tau_*$. The linking function parameter values used are given in Table 3.

find that the transmission rate due to contacting an infectious individual during the acute phase as being two orders of magnitude larger than the order of magnitude of the transmission rate corresponding to coming in contact with a carrier-infected individual.

After storing solution vectors for system (1), we can approximate $\mathcal{R}_{A0}$ by using trapezoidal rule to approximate the first integral given in (11) over interval $[0, \tau_{end}]$.

Now, the stored vectors for the carrier system (2) uses the initial values set to align with the beginning of the acute phase, so for approximating $\mathcal{R}_{C0}$, we use the trapezoid rule to approximate the second integral given in (11) over the interval $[\tau_*, \hat{\tau}_{end}]$ where τ_* is the time in which $P_C(\tau_*) < 10^{-4}$ (which estimates the start of the carrier phase). Using these methods and the calibrated parameter values described in Table 3, we have that $\mathcal{R}_{A0} \approx 15.6426$, $\mathcal{R}_{C0} \approx 7.3761$, and $\mathcal{R}_0 \approx 23.9187$.

In Subfigure 5a, we have that an infected individual experiences an increased probability of pathogen clearance in the bloodstream during days 5-8, and is over 99% likely to have pathogen clearance in the bloodstream by 7.6 days after infection. In Subfigure 5b, we have the plot of the probability of pathogen clearance in the tonsils during the carrier phase run over 750 days to get a clearer picture of the shape of the function. From this plot, we have that a carrier-infected individual is about 76.68% likely to recover by 243 days (after becoming a carrier) and over 99% likely to recover by day 395 days (after becoming a carrier). In Figure 5, we have plots of the transmission rates $\beta(\tau)$ and $\beta_C(\hat{\tau})$. Observe that value of the function $\beta(\tau)$ (at the time when $\beta(\tau)$ peaks) is two orders of magnitude larger than the value of $\beta_C(\hat{\tau})$ (at the beginning of the carrier stage), which aligns with what was observed in Jolles et al. (2021).

Epidemiological parameters w, ρ, and d are chosen to align those used in Jolles et al. (2021) while the remaining parameters, the birth rate Λ and the carrying capacity K, are adjusted to match $\mathcal{R}_0$.

4.2 Numerical results and epidemiological implications

In Figure 6, we have logarithmic plots of the classes $M(t)$, $S(t)$, $I(t)$, $C(t)$, and $R(t)$ during the first 500 days, and in the Appendix, we present Figure 12 (and Figure 13), which gives the log plots (and regular plots) of each compartment and the corresponding endemic steady state solution over the span of 2000 days to illustrate that the numerical solution to our model is approaching the endemic equilibrium.

As shown in Figure 6, we see that the replenishing of new susceptible individuals (red) and the presences of carrier-infected individuals (blue) are the driving factors for FMD disease persistence. These results (which is illustrated in the gray region) align with what was observed in Jolles et al. (2021). They considered two mechanisms for persistence of FMDV: (1) FMDV might be maintained as "typical childhood infections" do, where the elder born calves of one year spark an epidemic in the earliest born of the following cohorts, and (2) the presence of persistently-infected buffalo. In the gray shaded region of Figure 6, we have the maternally immune (magenta and dashed) steadily increasing due to new births. The susceptible population (which began with 100,000 individuals) drops to being as low as 4,282 individuals by day 26. This leads to the acute infected population (in the cyan and dashed plot line) peaking to having over 72,900 individuals by day 16. By day 30, carrier-infectious class peaks to having more than 95,000 individuals. By day 33 the acute-infected class drops to as low as 270 individuals and this is largely due to many acute-infected individuals quickly transitioning to either class $C(t)$ or $R(t)$ (green). Class $C(t)$ does not drop as significantly as class $I(t)$ and this is because the carrier stage is significantly longer than the acute stage. From days 26 to 50, we do not see the susceptible population fading out

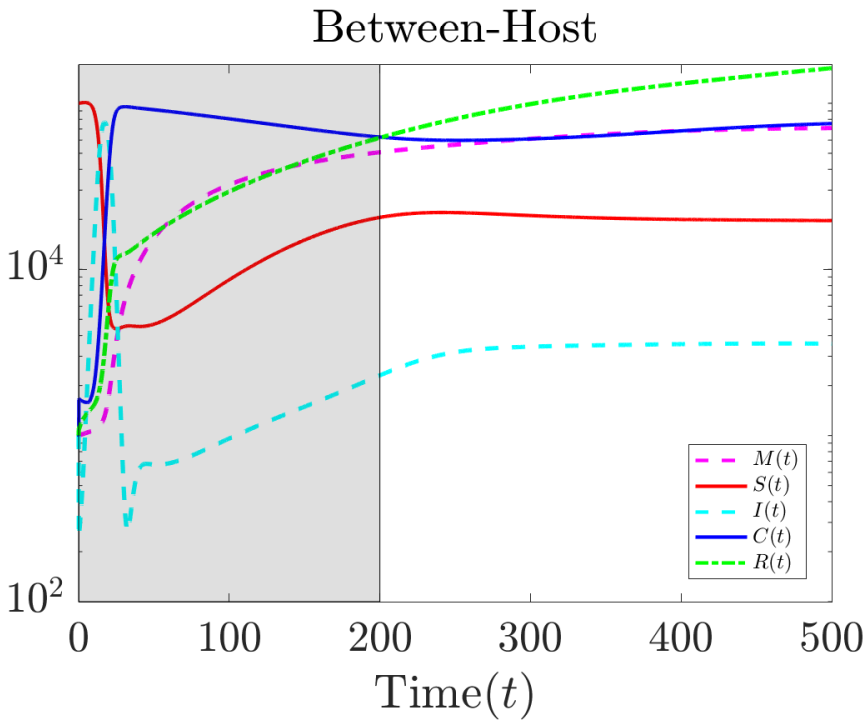

Fig. 6: Logarithmic plots of model compartments $M(t)$, $S(t)$, $I(t)$, $C(t)$, and $R(t)$. The shaded region shows that the susceptible population does not fade out due to new births. New susceptible individuals and the presence of carrier-infected individuals lead to a re-emergence of acute-infected individuals.

but rather remaining somewhere near 4282 to 4682 individuals. This phenomenon is likely due to births of new susceptible individuals and/or due to individuals in class $M(t)$ entering class $S(t)$ through waning immunity. From days 50 to 200, we observe a steady increase in the numbers of susceptible individuals, and also a similar rate of increase in class $I(t)$ at this time. By day 250, there are 3,170 acute infected individuals, and we do not see any significant declines in class $I(t)$ during time interval $[250, 500]$.

5 Impact of within-host parameters on $\mathcal{R}_0$

Sensitivity analysis (SA) is a tool that helps one quantifiably assess the impact of changes in model parameters on the infection dynamics, which can help one measure the expected efficacy of disease control strategies. In this section, we use SA method for multi-scale models developed in our prior work Gulbudak et al. (2022) to investigate the impact of within-host parameters on $\mathcal{R}_0$.

The elasticity or normalized forward sensitivity index of a quantity of interest (QOI) q (in our case, q is the basic reproduction $\mathcal{R}_0$ for the original system (8)) to

a parameter of interest (POI) p (such as immunological scale parameter viral growth rate r_A) can be defined as the ratio of relative change in the variable to the relative change in the parameter:

$$\gamma_p^q = \frac{\partial q}{\partial p} \times \frac{p}{q}.$$

Parameter	Sensitivity Analysis Range
	Parameters for acute infectious
b	$[0.09, 1]$
K_A	$[1, 12]$
r_A	$[1, 10]$
θ	$[10^{-6}, 0.1]$
μ	$[10^{-6}, 0.2]$
ξ	$[0.1, 4]$
ψ	$[10^{-2}, 0.7]$
Ω	$[0.1/21.23, 2/21.23]$
ω	$[10^{-3}, 0.5]$
	Parameters for carriers
a	$[0, 0.1]$
b_C	$[0.09, 1]$
K_C	$[1, 12]$
K_T	$[1, 12]$
r_C	$[1, 10]$
δ	$[0.00005, 0.017]$
η	$[10^{-5}, 0.1]$
θ_C	$[10^{-6}, 0.1]$
μ_C	$[10^{-6}, 0.2]$
ν	$[0.0025, 5.25]$
ξ_C	$[0.1, 4]$
ψ_C	$[10^{-2}, 0.7]$
Ω_C	$[0.1/21.23, 2/21.23]$
ω_C	$[10^{-3}, 0.5]$

Table 5: Ranges for parameters used in sensitivity analysis. Note parameter a is only being varied in the within-carrier model.

In our numerical experiments, we compute the sensitivity index $\gamma_p^{\mathcal{R}_0}$ when a within-host parameter p is set to a value around a baseline parameter value (see details in Appendix C). The parameters of interest and the ranges of parameters are given in Table 5. We rank the sensitivity index at the baseline values in Table 6 and observe the followings:

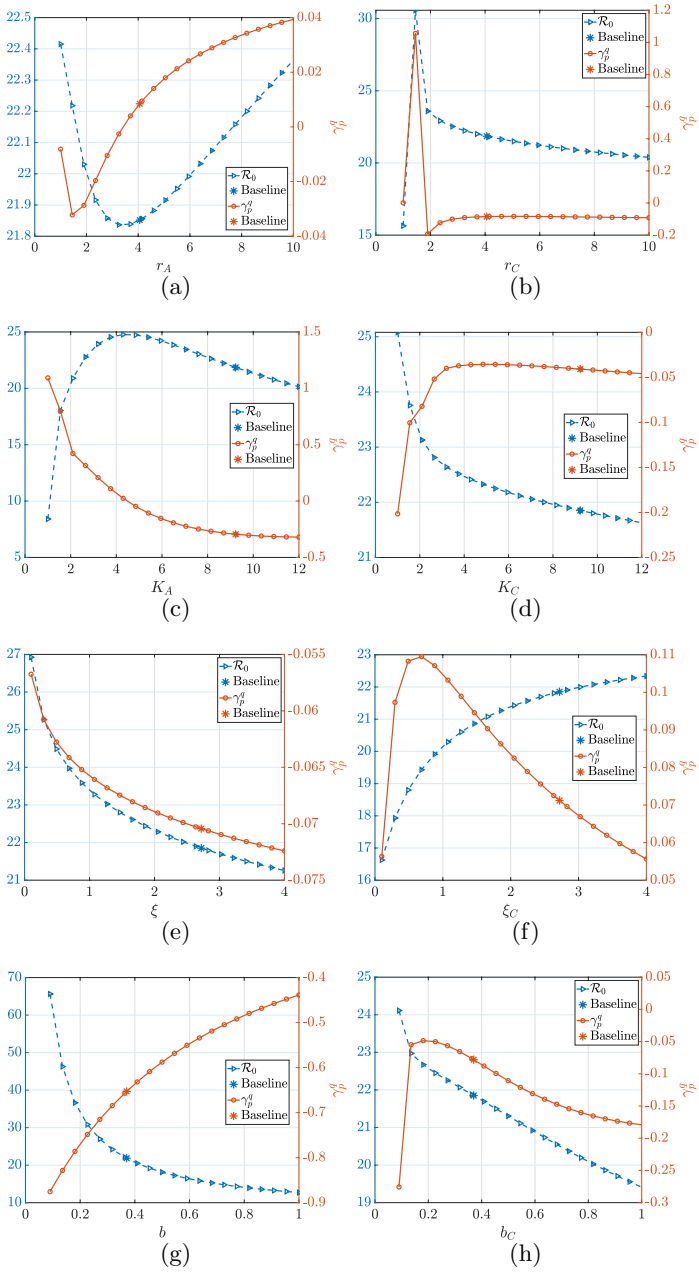

Fig. 7: Impact of viral and immunological parameters (r_A, r_C, K_A, K_C, ,ξ, ξ_C, b, and b_C) on $\mathcal{R}_0$. The virus-immune kinetics-dependent epidemiological reproduction number, $\mathcal{R}_0$ (left y-axis, blue curve) along with the response curves for the extended SA, $\gamma_p^{\mathcal{R}_0}$ (right y-axis, red curve) are plotted against the immune parameter values p over a range of values (see Table 5) the baseline estimates (see Table 3).

Rank	Parameter	$\gamma_p^{\mathcal{R}_0}$	Rank	Parameter	$\gamma_p^{\mathcal{R}_0}$
1	b	-0.653	13	θ	0.00117
2	K_T	0.338	14	θ_C	$7.43 \cdot 10^{-4}$
3	η	-0.307	15	ψ_C	$5.88 \cdot 10^{-4}$
4	K_A	-0.294	16	ψ	$3.39 \cdot 10^{-4}$
5	r_C	-0.0843	17	μ_C	$-1.93 \cdot 10^{-4}$
6	b_C	-0.0781	18	μ	$-1.15 \cdot 10^{-4}$
7	ν	0.0747	19	Ω_C	$4.87 \cdot 10^{-5}$
8	ξ_C	0.0712	20	Ω	$3.61 \cdot 10^{-5}$
9	ξ	-0.0704	21	ω	$-2.04 \cdot 10{-}5$
10	K_C	-0.0408	22	ω_C	$-1.94 \cdot 10^{-5}$
11	r_A	0.00848	23	a	0
12	δ	0.0071			

Table 6: Parameters and their sensitivity index ranked from most to least impactful. Note that the sensitivity index $\gamma_a^{\mathcal{R}_0} = 0$ because our baseline value for a is 0.

- All parameters corresponding to the innate immune response (at baseline values) had the least impact on $\mathcal{R}_0$. These results suggest that the innate immune response's performance on targeting the pathogen is least efficacious.
- At the baseline (estimated) values of the within-host immune parameters for both the acute and carrier stage, the within-host adaptive response activation rate during the acute phase b (with baseline value being 0.37) has the largest impact on $\mathcal{R}_0$: 1% increase in b causes a 0.653% reduction in $\mathcal{R}_0$. This suggests that the most efficient control measures are the ones that boost the adaptive immune response.
- The within-host pathogen carrying capacity in the tonsils during the carrier phase, K_T (with baseline parameter value 8) has the second largest impact on $\mathcal{R}_0$: 1% increase in K_T causes a 0.338% increase in $\mathcal{R}_0$.
- The decay rate of the pathogen in the tonsils, η, at the baseline parameter value 0.008, had the third largest impact on $\mathcal{R}_0$: 1% increase in η causes a 0.307% reduction in $\mathcal{R}_0$.

In Figures 7 and 8, we provide plots of the sensitivity index (in red) when a within host parameter p is varied and plots of the resulting $\mathcal{R}_0$ (in blue and with baseline value starred). Note that Figure 7 is organized to have the subfigures on the left-hand side correspond to within-acute parameters, while the right subfigures correspond to the within-carrier parameters. The figures corresponding to the impact of the innate immune response parameters (except for parameter a) on $\mathcal{R}_0$ are given in the Appendix (see Figure 14) since they were the least impacting on $\mathcal{R}_0$. From an immunological standpoint, it makes sense for the innate response parameters to not be as effective in changing $\mathcal{R}_0$ in comparison to the adaptive immune response since the primary role of the innate immune response is to send alarm signals that lead to the production of the adaptive immune response.

In subfigure 7g, we also observe that increasing the adaptive immune response activation rate, b, during the acute stage leads to a decrease in $\mathcal{R}_0$. As mentioned above, the parameter b has the largest impact on $\mathcal{R}_0$ at the baseline parameter values.

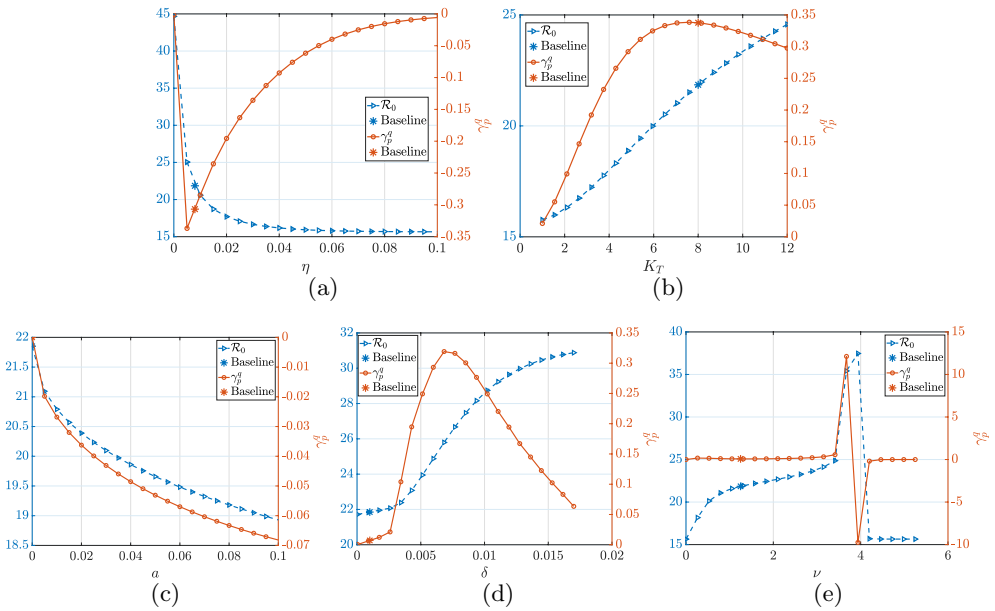

Fig. 8: Impact of within-carrier parameters ν, η, K_T, a, δ on $\mathcal{R}_0$. The immune-response-dependent epidemiological reproduction number, $\mathcal{R}_0$ (left y-axis, blue curve) along with the response curves for the extended SA, $\gamma_p^{\mathcal{R}_0}$ (right y-axis, red curve) are plotted against the immune parameter values p over a range of values (see Table 5) the baseline estimates (see Table 3). In subfigure (e) the SA results for ν exhibit unusual behavior when $\nu \in [3.41337, 4.2005]$. In subfigure 9a, reran sensitivity analysis results for ν but over a finer partition of $[3.41337, 4.2005]$.

Our SA results corresponding to parameter b align with our prior analysis on the acute stage of the disease (Macdonald et al., 2022). In our prior work, we observe a strong correlation between the adaptive immune response activation rates with the acute infection time period and find that this correlation to be one of the key influences on $\mathcal{R}_0$. In subfigure 7h, we observe that increasing the adaptive immune response activation rate during the carrier phase, b_C, also leads to a decrease in $\mathcal{R}_0$. Moreover, the parameter b_C is ranked as having the sixth largest impact on $\mathcal{R}_0$ at the estimated baseline values. Since the adaptive response activation rate during the carrier phase has an impact on the reduction of $\mathcal{R}_0$, continual application of a control that boosts the adaptive immune response during the carrier stage should have an epidemiological impact on reducing the spread.

The rankings of impact that the within-host carrying capacity in tonsils K_T and the killing rate of the pathogen in the tonsils η suggest that the pathogen load in the tonsils plays a crucial role at the epidemiological scale and control measures that target killing the viral load in the tonsils should be investigated. It is worth noting that such result may be a direct consequence of the formulation of the linking functions $\beta_C(\hat{\tau})$ and $\alpha(\hat{\tau})$, which should be validated with data.

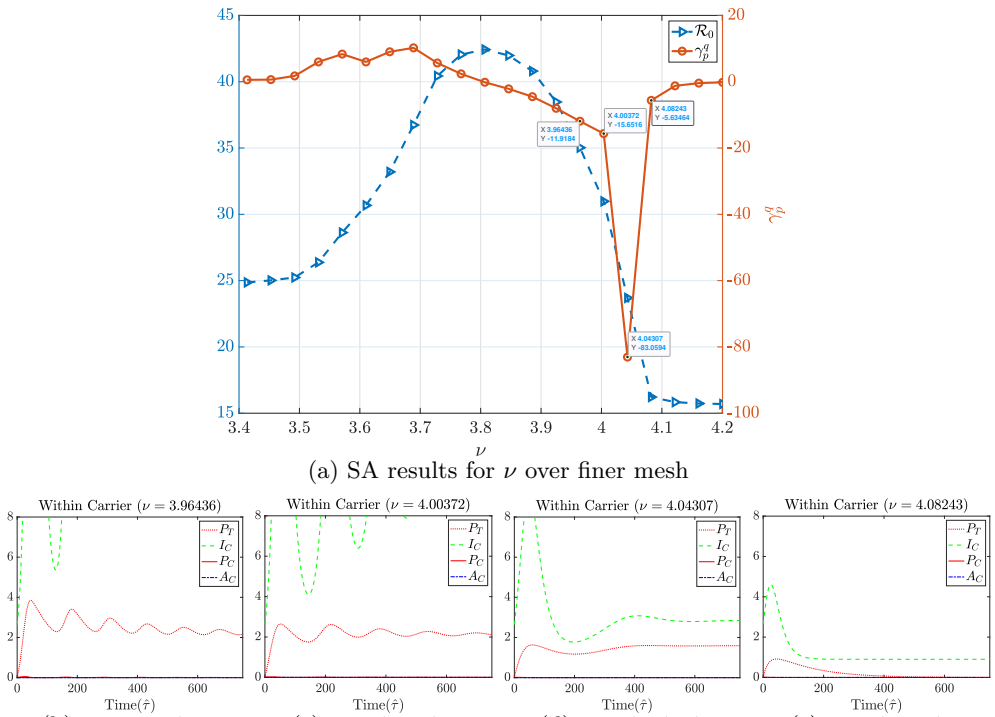

(a) SA results for ν over finer mesh

(b) $\nu = 3.96436$ (c) $\nu = 4.00372$ (d) $\nu = 4.04307$ (e) $\nu = 4.08243$

Fig. 9: Sensitivity analysis results of ν alongside the within-carrier solutions. In subfigure(a) we present the sensitivity analysis results to show that $\mathcal{R}_0$ is smooth on interval $\nu \in [3.41337, 4.2005]$. There is a dip in the sensitivity index at $\nu = 4.04307$. In subfigures(b)-(e), we display solutions to the within-carrier model (2) with $\nu \in \{3.96436, 4.00372, 4.04307, 4.08243\}$ and all other parameters set as described in Table 3. When $\nu = 3.96436, 4.00372$, and 4.04307 the solutions are converging to the the pathogen-persisting interior equilibrium $\mathcal{E}_2$, and when $\nu = 4.08243$ the solution is converging to the pathogen-free equilibrium $\mathcal{E}_0$ (See Appendix Subsection D Figure 15 which displays the same within-carrier simulations but over a longer time period to illustrate the convergence). The dip in the sensitivity analysis results corresponds to the immunological basic reproduction number switching from being $\mathscr{R}_0 > 1$ to $\mathscr{R}_0 < 1$. Observe also the computed epidemiological $\mathcal{R}_0$ when $\nu = 4.08243$ is close to $\mathcal{R}_{A0}$.

In subfigures 7a-7b, we have the sensitivity index of the viral replication rate in the blood during the acute phase r_A and the sensitivity index of the viral replication rate in the blood during the carrier phase r_C. In our SA results, we numerically observe that an increase in $r_A > 0$ leads to an increase in $\mathcal{R}_0$. In our prior work Macdonald et al. (2022), we observe that the viral growth rate have a negative correlation with the latent period, in that buffalo having fast-growing viral populations transfer to the infectious class more rapidly. As mentioned in other works (Grassly and Fraser, 2008; Sartwell, 1995; Fine, 2003) short incubation periods plays a significant role in

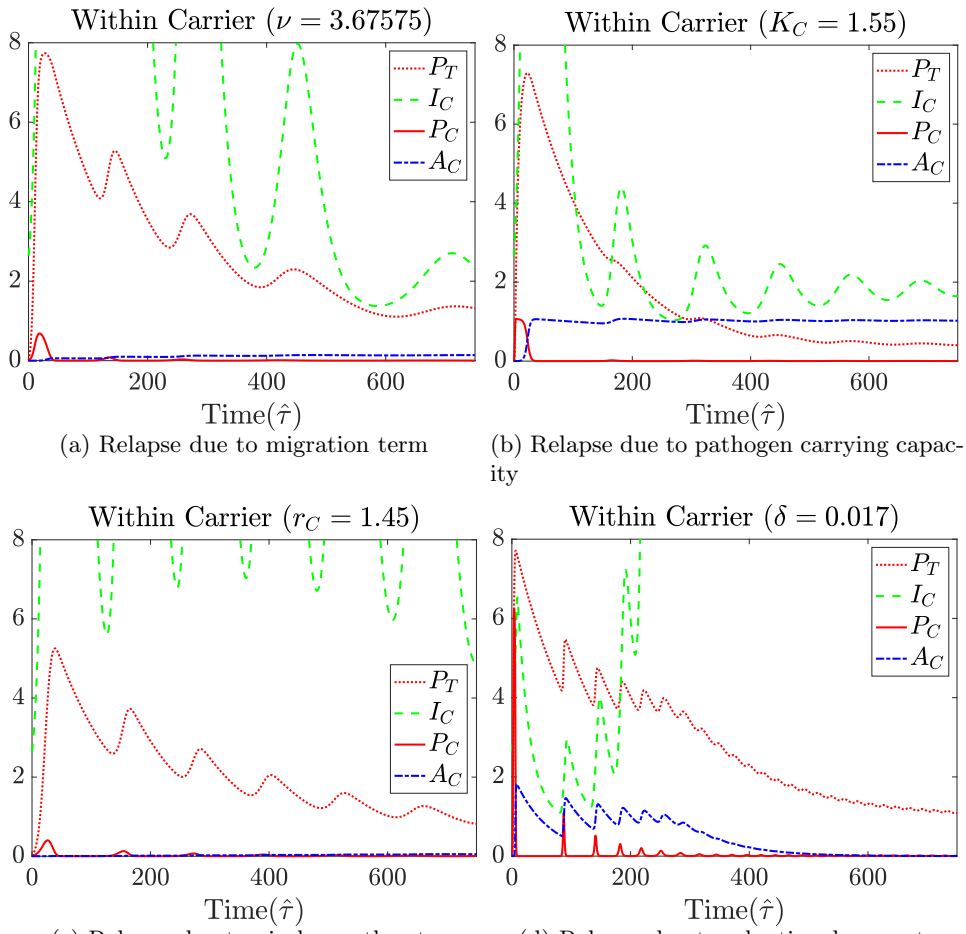

(a) Relapse due to migration term

(b) Relapse due to pathogen carrying capacity

(c) Relapse due to viral growth rate

(d) Relapse due to adaptive decay rate

Fig. 10: Instances of viral relapse from the carrier model (2) These subfigures demonstrate how the within-carrier model can display viral relapse. For each simulation, one of the within-carrier parameters was set to a different value, as described in the subfigure titles, while the remaining within-carrier parameters were set to the baseline parameter values (see Table 3).

the rapid spread of highly transmissible pathogens. This could explain why the viral growth rate has a significant impact on $\mathcal{R}_0$.

An interesting result is that increases in r_C leads to decreases in $\mathcal{R}_0$. This could be suggesting that a higher viral replication rate could contribute to a shorter carrier stage. This can occur because increasing the viral growth rate can result in a shorter duration for which the pathogen remains in the bloodstream (due to increased levels in the adaptive immune response). The shorter the duration of the viral load in the bloodstream, the fewer opportunities for the pathogen to migrate to the tonsils.

However, our SA results corresponding to varying r_C is only measuring how such a parameter change influences $\mathcal{R}_0$ via influencing $\mathcal{R}_{C0}$. The results presented in subfigure 7a indicates a significant drawback of what happens when a high viral replication rate occurs during the acute phase. More specifically the higher the viral growth rate, the higher the transmission level during the acute phase. It is worth mentioning that in the within carrier model (2) the pathogen migration term ν in a way can be viewed a viral replication rate in the tonsils. In Table 6, we see that at the baseline parameter values, ν behaves similarly to the viral replication rate in the bloodstream during the acute phase, r_A, in that an increase in ν leads to an increase in $\mathcal{R}_0$, but ν has a higher impact in comparison to r_A.

In subfigure 8e, the graphs of the computed sensitivity index and $\mathcal{R}_0$ appear to be nonsmooth when $\nu \in [3.41337, 4.2005]$. In particular, when $\nu = 3.67575$ the sensitivity index $\gamma_\nu^{\mathcal{R}_0}$ jumps to 12.12 and $\mathcal{R}_0$ increases to 35.4174. When $\nu = 3.93812$, $\gamma_\nu^{\mathcal{R}_0}$ drops to -9.74427 but $\mathcal{R}_0 = 37.467$. The sensitivity index being negative here should implies that $\mathcal{R}_0$ should be decreasing near $\nu = 3.93812$. We can then infer that $\mathcal{R}_0$ peaks at some value $\nu \in (3.67575, 3.93812)$. We support this inference by rerunning the sensitivity analysis simulations for ν over a finer partition of $[3.41337, 4.2005]$, and the results are given in subfigure 9a. The graph of the computed $\mathcal{R}_0$ given in subfigure 9a is smooth, but the graph of the sensitivity index does not look smooth near $\nu = 4.04307$. Note that using a finer partition does not improve this characteristic. This is because there is some $\nu \in (4.04307, 4.08243)$, for which the pathogen-free equilibrium $\mathcal{E}_0$ (expression given in Table 2) is changing from being unstable to being locally asymptotically stable (Recall, that at the baseline parameter values $\mathcal{E}_0$ is unstable.). The immunological reproduction number $\mathscr{R}_0$ (3) is approximately 1.00307 and 0.99341 when $\nu = 4.04307$ and $\nu = 4.08243$ (respectively). In Figure 9 we numerically solved for the within carrier model (2) for varying values of $\nu \in \{3.96436, 4.00372, 4.04307, 4.08243\}$. When $\nu = 3.96436$, we observe viral relapse in the tonsils within the first 750 days. Because the transmission rate $\beta_C(\hat{\tau})$ depends on the pathogen load in the tonsils, these instances of viral relapse lead to a larger value for $\mathcal{R}_0$. As we increase ν to 4.00372 and 4.04307, we see the oscillatory behavior in the pathogen load for the tonsils dissipate and a decrease in $\mathcal{R}_0$ is observed. Lastly when $\nu = 4.08243$, we see that the solution is converging to the $\mathcal{E}_0$, and $\mathcal{R}_0 = 16.2211$.

Our results presented in Figure 10 indicate that the carrier model (2) is more likely to display viral relapse in comparison to the acute model (1). Changes in the within-carrier parameter values can have an impact on immunological quantities (i.e., $\mathscr{R}_0$, $\mathscr{R}_1$, and $\mathscr{R}_2$, which are given in Table 1) that determine the stability of a steady state solution to system (2). The duration of the carrier phase for an FMD infected-buffalo varies from months to years (Stenfeldt C, 2020; Shikumwifa, 2022). Instances of viral relapse could explain why some buffalo undergo a longer duration of the carrier phase in the sense that viral relapse would delay the process in clearing the pathogen in the tonsils. In the context of immunology, instances of viral relapse could arise in a carrier-infected buffalo if some of the viral particles within the tonsils were to drip back into the bloodstream; however, to our best knowledge no field studies are investigating such a phenomenon.

6 Discussion

The foot-and-mouth disease (FMD) is a highly contagious disease that spreads among buffalo population, and a major concern of FMD is in how persistently infected hosts can cause potential obstacles in disease eradication in South African territories. We formulate a novel immuno-epidemiological model of FMD in African buffalo to investigate the role of carrier transmission on the disease dynamics. This model takes both the acute and carrier stages of the disease into consideration by incorporating two within-host models that capture the viral and immune dynamics within an FMD infected buffalo experiencing only acute or both phases, and by coupling these models to a time-since-infection age structured epidemiological model.

In analyzing the within-host model of carrier-infected buffalo, we define an immunological basic reproduction number, $\mathscr{R}_0$, that also serves as a threshold condition for local stability of a pathogen-free equilibrium. Additionally, we present existence and stability conditions for two pathogen persisting equilibria. Furthermore, we analyze the immuno-epidemiological multi-scale model. We first define a within-host viral-immune kinetics dependent basic reproduction number, $\mathcal{R}_0$, and later show that it serves as a threshold condition for the local stability of the disease-free equilibrium and existence of the endemic equilibrium. We also analytically show that the epidemiological model always displays forward bifurcation for specific between-host parameters, excluding the possibility of backward bifurcation.

Numerical results indicate that two mechanisms drive the persistence of FMD. One mechanism pertains to the role of FMDV persistence due to carrier-infected buffalo remaining in the population. The second mechanism is that FMDV operates as a childhood disease in the sense that carrier and acute infected populations of a specific strain remain in the population to where they can introduce that strain to newly birthed calves. Such results align with Jolles et al. (2021). We apply sensitivity analysis to better understand the impact of within-host parameters on $\mathcal{R}_0$. Sensitivity analysis suggests that the most efficient control measures are the ones that prioritize boosting of the adaptive immune response and such measures should be applied even while individuals are carriers. Through our sensitivity analysis results, we also recognize that solutions to the within-host carrier model can display viral relapse for varying values of the parameters. Viral relapse could be one of the reasons why buffalo remain infected for longer periods of times.

Further analysis on the foot-and-mouth disease can be useful in elucidating how fast transmitting and evolving diseases spread among a population and how to manage such outbreaks. A future research endeavor of ours is to validate the immunological carrier model with data. In addition, we aim to analyze the practical identifiability of these parameters. We are also interested in formulating and analyzing nested immuno-epidemiological coinfection models for FMD and in investigating the application of immunological control strategies by applying optimal control theory to the within-acute and within-carrier model to where we can also investigate the epidemiological impacts that such strategies have on curtailing the spread of the disease.

7 Acknowledgements

We would like to thank Anna Jolles (Oregon State University), Brianna Beechler (Oregon State University), Joshua Caleb Macdonald (Tel Aviv University), Simon Gubbins (The Pirbright Institute), Jan Medlock (Oregon State University), and Maia Martcheva (University of Florida) for conversations that were helpful to us while conducting this research.

8 Declarations

Funding: Author H.G. is supported by a U.S. NSF RAPID grant (no. DMS-2028728) and NSF grant (no. DMS1951759), and by a grant from the Simons Foundation/S-FARI. Ongoing work is supported by the NSF-NIH-NIFA Ecology and Evolution of Infectious Disease (number 2208087).
Competing Interests: The authors have no relevant financial and non-financial interests to disclose.

Appendix A Analyses of the within-carrier model

In analyzing the within-carrier system (2), we assume $a = 0$ to align with results in fitting the system. Thus the equilibria of the within-carrier system are given by the solutions of

$$0 = \nu P_C \left(1 - \frac{P_T}{K_T}\right) - \eta P_T \tag{A1a}$$

$$0 = \Omega_C + \frac{\psi_C P_C}{\omega_C + P_C} I_C - \mu_C I_C \tag{A1b}$$

$$0 = \left[r_C \left(1 - \frac{P_C}{K_C}\right) - \theta_C I_C - \xi_C A_C - \nu\right] P_C \tag{A1c}$$

$$0 = b_C A_C P_C - \delta A_C. \tag{A1d}$$

The generic Jacobian of the system is

$$J(\mathcal{E}) = \begin{pmatrix} -\frac{\nu P_C}{K_T} - \eta & 0 & \nu\left(1 - \frac{P_T}{K_T}\right) & 0 \\ 0 & \frac{\psi_C P_C}{\omega_C + P_C} - \mu_C & \frac{\omega_C \psi_C I_C}{(\omega_C + P_C)^2} & 0 \\ 0 & -\theta_C P_C & r_C\left(1 - 2\frac{P_C}{K_C}\right) - \theta_C I_C - \xi_C A_C - \nu & -\xi_C P_C \\ 0 & 0 & b_C A_C & b_C P_C - \delta \end{pmatrix}.$$

The computed Jacobian presented above will be used for proving Theorems 2.1-2.3, which will be presented in the following subsections.

A.1 Stability analysis of the pathogen-free equilibrium

Theorem 2.1. *The pathogen-free equilibrium*

$$\mathcal{E}_0 = \left(0,\ \frac{\Omega_C}{\mu_C},\ 0,\ 0\right),$$

which always exists, is locally asymptotically stable when

$$\mathscr{R}_0 < 1$$

and unstable when

$$\mathscr{R}_0 > 1.$$

Proof. The Jacobian evaluated at $\mathcal{E}_0$ is

$$J(\mathcal{E}_0) = \begin{pmatrix} -\eta & 0 & \nu & 0 \\ 0 & -\mu_C & \dfrac{\psi_C \Omega_C}{\mu_C \omega_C} & 0 \\ 0 & 0 & r_C - \dfrac{\theta_C \Omega_C}{\mu_C} - \nu & 0 \\ 0 & 0 & 0 & -\delta \end{pmatrix},$$

which has eigenvalues $\lambda_1 = -\eta$, $\lambda_2 = -\mu_C$, $\lambda_3 = -\delta$, and $\lambda_4 = r_C - \frac{\theta_C \Omega_C}{\mu_C} - \nu$. Since $\lambda_1,\ \lambda_2,\ \lambda_3 < 0$, the stability of $\mathcal{E}_0$ is determined by the sign of λ_4.

We can rewrite λ_4 as follows:

$$\lambda_4 = r_C \left(1 - \frac{1}{\mathscr{R}_0}\right),$$

where

$$\mathscr{R}_0 = \frac{r_C}{\theta_C \frac{\Omega_C}{\mu_C} + \nu}.$$

Therefore, $\mathcal{E}_0$ is locally asymptotically stable when

$$\mathscr{R}_0 < 1$$

and unstable when

$$\mathscr{R}_0 > 1.$$

□

A.2 Stability analysis of the pathogen-persisting boundary equilibrium

We next consider the possibility of a boundary pathogen-persisting equilibrium $\mathcal{E}_1^*$. In this case, the adaptive immune response is absent, i.e., $A_C^* = 0$. From (A1a), we have

$$P_T^* = \frac{\nu P_C^*}{\frac{\nu P_C^*}{K_T} + \eta} = \frac{\nu K_T P_C^*}{\nu P_C^* + \eta K_T}.$$

From (A1b), we have

$$I_C^* = \frac{\Omega_C}{\mu_C - \frac{\psi_C P_C^*}{\omega_C + P_C^*}} = \frac{\Omega_C(\omega_C + P_C^*)}{\mu_C(\omega_C + P_C^*) - \psi_C P_C^*},$$

which exists when $\mu_C(\omega_C + P_C^*) - \psi_C P_C^* > 0$. Substituting the above expression into (A1c), we obtain

$$\begin{aligned}
0 &= r_C\left(1 - \frac{P_C^*}{K_C}\right) - \theta_C\left(\frac{\Omega_C(\omega_C + P_C^*)}{\mu_C(\omega_C + P_C^*) - \psi_C P_C^*}\right) - \nu \\
&= r_C(K_C - P_C^*) - \theta_C K_C\left(\frac{\Omega_C(\omega_C + P_C^*)}{\mu_C(\omega_C + P_C^*) - \psi_C P_C^*}\right) - K_C\nu \\
&= K_C(r_C - \nu) - r_C P_C^* - \frac{K_C\theta_C\Omega_C(\omega_C + P_C^*)}{\mu_C(\omega_C + P_C^*) - \psi_C P_C^*} \\
&= K_C(r_C - \nu) - r_C P_C^* - \frac{K_C\theta_C\Omega_C(\omega_C + P_C^*)}{\mu_C\omega_C + (\mu_C - \psi_C)P_C^*} \\
&= K_C(r_C - \nu)\mu_C\omega_C + K_C(r_C - \nu)(\mu_C - \psi_C)P_C^* - r_C\mu_C\omega_C P_C^* - r_C(\mu_c - \psi_C)(P_C^*)^2 \\
&\quad - K_C\theta_C\Omega_C\omega_C - K_C\theta_C\Omega_C P_C^* \\
&= -r_C(\mu_C - \psi_C)(P_C^*)^2 + [K_C(r_C - \nu)(\mu_C - \psi_C) - r_C\mu_C\omega_C - K_C\theta_C\Omega_C]P_C \\
&\quad + K_C[(r_C - \nu)\mu_C - \theta_C\Omega_C]\omega_C
\end{aligned}$$

$$0 = \hat{A}_2(P_C^*)^2 + \hat{A}_1 P_C^* + \hat{A}_0,$$

where

$$\hat{A}_2 = -r_C(\mu_C - \psi_C), \tag{A2}$$

$$\hat{A}_1 = K_C\left[(r_C - \nu)(\mu_C - \psi_C) - \theta_C\Omega_C\right] - r_C\mu_C\omega_C, \tag{A3}$$

$$\hat{A}_0 = K_C\omega_C[(r_C - \nu)\mu_C - \theta_C\Omega_C]. \tag{A4}$$

We denote $f(P_C)$ as being the following quadratic polynomial

$$f(P_C) = \hat{A}_2(P_C)^2 + \hat{A}_1 P_C + \hat{A}_0, \tag{A5}$$

with coefficients being defined in equations (A2)-(A4). Before discussing the theorem of existence, uniqueness, and stability of a pathogen-persisting boundary equilibrium, we present the following lemma.

Lemma A.1. *The following hold true:*
Case 1: If $\mathscr{R}_0 < 1$ and $\mu_C > \psi_C$, then Equation (A5) has no positive roots.
Case 2: If $\mathscr{R}_0 < 1$ and $\mu_C < \psi_C$, then Equation (A5) has one positive root.
Case 3: If $\mathscr{R}_0 > 1$ and $\mu_C > \psi_C$, then Equation (A5) has one positive root.
Case 4: If $\mathscr{R}_0 > 1$ and $\mu_C < \psi_C$, then Equation (A5) has either two positive roots or no positive roots.

Proof. Verification of each case follows directly from Descartes' Rule of Signs and a couple of observations. First we can rewrite $\hat{A}_1$ and $\hat{A}_0$ as follows:

$$\hat{A}_1 = K_C \left[r_C \mu_C \left(1 - \frac{1}{\mathscr{R}_0}\right) - \psi_C (r_C - \nu) \right] - r_C \mu_C \omega_C \tag{A6}$$

$$\hat{A}_0 = r_C \omega_C \mu_C K_C \left(1 - \frac{1}{\mathscr{R}_0}\right). \tag{A7}$$

Additionally, we have that $\mathscr{R}_0 > 1$ implies that $r_C > \nu$.
Case 1: Assume $\mathscr{R}_0 < 1$ and $\mu_C > \psi_C$, then it follows that $\hat{A}_2 < 0$ and $\hat{A}_0 < 0$. For determining the sign of $\hat{A}_1$ we consider to subcases.
Subcase 1a) Assume $r_C < \nu$. From Equation (A3) the term $(r_C - \nu)(\mu_C - \psi_C) < 0$. This allows us to deduce that $\hat{A}_1 < 0$, and (by Descartes' Rule of Signs) Equation (A5) has no positive roots.
Subcase 1b) Assume $r_C \geq \nu$. From Equation (A6) we have $r_C(1 - 1/\mathscr{R}_0) < 0$ since $\mathscr{R}_0 < 1$ and the other two terms are clearly negative. We can deduce that $\hat{A}_1 < 0$ and so Equation (A5) has no positive roots.
Case 2) Assume $\mathscr{R}_0 < 1$ and $\mu_C < \psi_C$, then $\hat{A}_2 > 0$ and $\hat{A}_0 < 0$. We can then deduce that Equation (A5) has exactly one positive root.
Case 3) Assume $\mathscr{R}_0 > 1$ and $\mu_C > \psi_C$. It then follows that $\hat{A}_2 < 0$ and $\hat{A}_0 > 0$, which allows us to deduce that Equation (A5) has exactly 1 positive root.
Case 4) Assume $\mathscr{R}_0 > 1$ and $\mu_C < \psi_C$. Then, it follows that $\hat{A}_2 > 0$, $\hat{A}_0 > 0$, $\hat{A}_1 < 0$. By Descartes' Rule of Signs Equation (A5) either has two positive roots or no positive roots. □

Theorem 2.2. *If one of the two following conditions below holds:*

1. *$\mathscr{R}_0 > 1$ and $\mu_C > \psi_C$.*
2. *$\mathscr{R}_0 > 1$, $\mu_C < \psi_C$, and the discriminant of the quadratic polynomial $f(P_C)$, $\hat{A}_1^2 - 4\hat{A}_0\hat{A}_2$, is positive,*

then there exists a unique pathogen-persisting boundary equilibrium $\mathcal{E}_1^*$. Moreover if $P_C^* < \frac{\delta}{b_C}$, then the pathogen persisting boundary equilibrium is locally asymptotically stable.

Proof. Before discussing conditions 1 and 2, we need to verify that the parameters set to satisfy cases 1 and 2 from Lemma A.1 (that is the cases in which $\mathscr{R}_0 < 1$) imply that the pathogen persisting boundary equilibrium does not exist. In order for the pathogen persisting boundary equilibrium to exist, we need $P_C^* > 0$ and $I_C^* > 0$. In Lemma A.1, we showed that if $\mathscr{R}_0 < 1$, and $\mu_C > \psi_C$, there is no positive root $P_C^* > 0$, so no boundary equilibrium arises from this case. In Lemma A.1, we showed that if $\mathscr{R}_0 < 1$ and $\mu_C < \psi_C$, then we have existence of exactly one positive root P_C^*. In order for steady state value I_C^* to also be positive, $\mu_C(\omega_C + P_C^*) - \psi_C P_C^* > 0$ or equivalently $P_C^* < \frac{\mu_C \omega_C}{\psi_C - \mu_C}$. We can use properties of quadratic polynomial f and the value of $f\left(\frac{\mu_C \omega_C}{\psi_C - \mu_C}\right)$ to show that this inequality does not hold when $\mathscr{R}_0 < 1$ and $\mu_C < \psi_C$. As mentioned in the proof of Lemma A.1, $\mathscr{R}_0 < 1$ and $\mu_C < \psi_C$ implies that $\hat{A}_2 > 0$ and $\hat{A}_0 < 0$. This implies that f is a parabola that opens up with y-intercept below the x-axis. Thus showing that the positive root of f satisfies $P_C^* < \frac{\mu_C \omega_C}{\psi_C - \mu_C}$ is equivalent to showing that $f\left(\frac{\mu_C \omega_C}{\psi_C - \mu_C}\right) > 0$. We evaluate $f\left(\frac{\mu_C \omega_C}{\psi_C - \mu_C}\right)$ with (A7), (A6), and (A2) substituted in for $\hat{A}_0$, $\hat{A}_1$, and $\hat{A}_2$ (respectively) and use algebra to simplify terms to get

$$f\left(\frac{\mu_C \omega_C}{\psi_C - \mu_C}\right) = \frac{K_C \psi_C \mu_C \omega_C \frac{r_C}{\mathscr{R}_0}\left(\frac{\nu \mathscr{R}_0}{r_C} - 1\right)}{\psi_C - \mu_C}. \tag{A8}$$

Note that sign of the numerator depends on the the sign of $(\nu \mathscr{R}_0 / r_C) - 1$. We use (3) to obtain:

$$\frac{\nu \mathscr{R}_0}{r_C} - 1 = \frac{\nu}{\theta_C \frac{\Omega_C}{\mu_C} + \nu} - 1 < 0.$$

Thus, the numerator for $f\left(\frac{\mu_C \omega_C}{\psi_C - \mu_C}\right)$ is always negative, and this holds true regardless of whether or not $\mathscr{R}_0$ is greater than or less than one. Since $\mu_C < \psi_C$, $f\left(\frac{\mu_C \omega_C}{\psi_C - \mu_C}\right) < 0$. Therefore, the positive root corresponding to the case in which $\mathscr{R}_0 < 1$ and $\mu_C < \psi_C$ does not satisfy $P_C^* < \frac{\mu_C \omega_C}{\psi_C - \mu_C}$ which allows us to deduce that no boundary equilibrium exists in this scenario.

In Lemma A.1, we showed that $\mathscr{R}_0 > 1$ and $\mu_C > \psi_C$ (this is Condition 1 from our theorem), then f has a unique positive root P_C^*. In order for the steady state value I_C^* to also be positive in this case, $P_C^* > \frac{\mu_C \omega_C}{\psi_C - \mu_C}$ which is immediately satisfied since the right hand side of the inequality is negative.

In Lemma A.1, we showed that $\mathscr{R}_0 > 1$ and $\mu_C < \psi_C$ implies that f has either two positive roots or no positive roots. In order to have positive roots the discriminant of quadratic polynomial f, that is $\hat{A}_1^2 - 4\hat{A}_2\hat{A}_0$, must be positive, which is why such inequality is also added to condition 2 of our theorem. Although we get existence of two positive roots in this scenario, the smaller positive root, which we denote as P_{C1}^*, is the only root that yields a positive steady state value for I_C^*. In order for I_C^* to be positive $P_C^* < \frac{\mu_C \omega_C}{\psi_C - \mu_C}$. If parameters are set to satisfy condition 2 of the theorem, f is a parabola that opens up with the y-intercept lying above the x-axis. We denote P_{C2}^* as being the larger positive root. Based upon the characteristics of f, the graph of $f(x) > 0$ should lie below the x-axis for any $P_{C1}^* < x < P_{C2}$ and the graph of $f(x)$ is above the x-axis for any $x < P_{C1}^*$ and any $x > P_{C2}^*$. From Equation (A8) we

have that $f\left(\frac{\mu_C\omega_C}{\psi_C-\mu_C}\right) < 0$ when $\mu_C < \psi_C$, which implies that $P^*_{C1} < \frac{\mu_C\omega_C}{\psi_C-\mu_C} < P^*_{C2}$. Therefore, the steady state value of the innate immune response,I^*_{C1}, corresponding to the smallest positive root P^*_{C1} is positive while the steady state value of the innate immune response corresponding to the larger positive root $I^*_{C2} < 0$. This tells us that for condition 2 we get existence of a unique pathogen persisting boundary equilibrium.

To analyze the stability of $\mathcal{E}^*_1$ we compute the Jacobian

$$J(\mathcal{E}^*_1) = \begin{pmatrix} -\dfrac{\nu P^*_C}{K_T} - \eta & 0 & \nu\left(1 - \dfrac{P^*_T}{K_T}\right) & 0 \\ 0 & \dfrac{\psi_C P^*_C}{\omega_C + P^*_C} - \mu_C & \dfrac{\omega_C\psi_C I^*_C}{(\omega_C + P^*_C)^2} & 0 \\ 0 & -\theta_C P^*_C & -\dfrac{r_C P^*_C}{K_C} & -\xi_C P^*_C \\ 0 & 0 & 0 & b_C P^*_C - \delta \end{pmatrix}.$$

The matrix $J(\mathcal{E}^*_1)$ has two eigenvalues

$$\lambda_1 = -\frac{\nu P^*_C}{K_T} - \eta, \quad \lambda_2 = b_C P^*_C - \delta.$$

The sign of λ_1 is negative and the sign of λ_2 is negative if $P^*_C < \frac{\delta}{b_C}$. To investigate the remaining eigenvalues, we first observe that the second diagonal entry of $J(\mathcal{E}^*_1)$ can be rewritten as $-\Omega/I^*_C$, since $I^*_C = \Omega_C(\omega_C + P^*_C)/(\mu_C(\omega_C + P^*_C) - \psi_C P^*_C)$. Then we consider the following submatrix

$$J_1 = \begin{pmatrix} -\frac{\Omega_C}{I^*_C} & \dfrac{\omega_C\psi_C I^*_C}{(\omega_C + P^*_C)^2} \\ -\theta_C P^*_C & -\frac{r_C P^*_C}{K_C} \end{pmatrix}.$$

We can determine the sign of the remaining eigenvalues by analyzing the trace of J_1 and the determinant of J_1. Observe $\mathrm{Tr}(J_1) = -\frac{\Omega_C}{I^*_C} - \frac{r_C P^*_C}{K_C} < 0$ and $\det(J_1) = \frac{\Omega_C r_C P^*_C}{I^*_C K_C} + \frac{\theta_C P^*_C \omega_C \psi_C I^*_C}{(\omega_C + P^*_C)^2} > 0$, which implies that the sign of the remaining eigenvalues are negative. This completes our proof. □

A.3 Stability analysis of the pathogen-persisting interior equilibrium

We now consider the pathogen-persisting interior equilibrium

$$\mathcal{E}^*_2 = (P^*_T,\ I^*_C,\ P^*_C,\ A^*_C),$$

where

$$
\begin{aligned}
P_T^* &= \frac{\nu K_T P_C^*}{\nu P_C^* + \eta K_T} = \frac{\nu K_T \delta}{\nu\delta + \eta b_C K_T}, \\
I_C^* &= \frac{\Omega_C(\omega_C + P_C^*)}{\mu_C(\omega_C + P_C^*) - \psi_C P_C^*} = \frac{\Omega_C}{\mu_C}\left(\frac{1}{1 - \frac{\psi_C P_C^*}{\mu_C(\omega_C + P_C^*)}}\right) = \frac{\Omega_C}{\mu_C}\left(\frac{1}{1-\mathscr{R}_1}\right), \\
P_C^* &= \frac{\delta}{b_C}, \\
A_C^* &= \frac{1}{\xi_C}\left[r_C\left(1 - \frac{P_C^*}{K_C}\right) - \frac{\theta_C \Omega_C(\omega_C + P_C^*)}{\mu_C(\omega_C + P_C^*) - \psi_C P_C^*} - \nu\right] \\
&= \frac{1}{\xi_C}\left(\frac{\theta_C \Omega_C}{\mu_C}\left(\frac{1}{1-\mathscr{R}_1}\right) + \nu\right)(\mathscr{R}_2 - 1)
\end{aligned}
$$

$$
\mathscr{R}_1 = \frac{\psi_C \frac{\delta}{b_C}}{\mu_C\left(\omega_C + \frac{\delta}{b_C}\right)} \text{ and } \mathscr{R}_2 = \frac{r_C\left(1 - \frac{\delta/b_C}{K_C}\right)}{\frac{\theta_C \Omega_C}{\mu_C}\left(\frac{1}{1-\mathscr{R}_1}\right) + \nu}.
$$

Theorem 2.3. *The pathogen-persisting interior equilibrium,* $\mathcal{E}_2^* = (P_T^*,\ I_C^*,\ P_C^*,\ A_C^*)$, *exists and is locally asymptotically stable if*

$$
\mathscr{R}_1 < 1 \text{ and } \mathscr{R}_2 > 1. \tag{7}
$$

Proof. The condition $\mathscr{R}_1 < 1$ ensures that I_C^* is positive, and the second condition $\mathscr{R}_2 > 1$ in the theorem ensures that A_C^* is positive. We now linearize 2 about this equilibrium. First, note that, as $P_C \neq 0$, (A1c) implies

$$
r_C\left(1 - \frac{P_C}{K_C}\right) - \theta_C I_C - \xi_C A_C - \nu = 0.
$$

Thus, the Jacobian evaluated at $\mathcal{E}_2^*$ is

$$
J(\mathcal{E}_2^*) = \begin{pmatrix}
-\frac{\nu P_C^*}{K_T} - \eta & 0 & \nu\left(1 - \frac{P_T^*}{K_T}\right) & 0 \\
0 & \frac{\psi_C P_C^*}{\omega_C + P_C^*} - \mu_C & \frac{\psi_C \omega_C I_C^*}{(\omega_C + P_C^*)^2} & 0 \\
0 & -\theta_C P_C^* & -\frac{r_C P_C^*}{K_C} & -\xi_C P_C^* \\
0 & 0 & b_C A_C^* & 0
\end{pmatrix}.
$$

One of the eigenvalues of $J(\mathcal{E}_2^*)$ is

$$
\lambda_1 = -\frac{\nu P_C^*}{K_T} - \eta,
$$

which is negative. We use $\mathscr{R}_1$ to rewrite the second diagonal entry of $J(\mathcal{E}_2^*)$, $\psi_C P_C^*/(\omega_C + P_C^*) - \mu_C$, as being $-\mu_C(1-\mathscr{R}_1)$. Consider the submatrix

$$J_2 = \begin{pmatrix} -\mu_C(1-\mathscr{R}_1) & \frac{\psi_C \omega_C I_C^*}{(\omega_c + P_C^*)^2} & 0 \\ -\theta_C P_C^* & -\frac{r_C P_C^*}{K_C} & -\xi_C P_C^* \\ 0 & b_C A_C^* & 0 \end{pmatrix}.$$

The remaining eigenvalues are the solutions of the following equation

$$\begin{vmatrix} \lambda + \mu_C(1-\mathscr{R}_1) & -\frac{\psi_C \omega_C I_C^*}{(\omega_c + P_C^*)^2} & 0 \\ \theta_C P_C^* & \lambda + \frac{r_C P_C^*}{K_C} & \xi_C P_C^* \\ 0 & -b_C A_C^* & \lambda \end{vmatrix} = 0.$$

By expanding the determinant, we have

$$\lambda^3 + a_1\lambda^2 + a_2\lambda + a_3 = 0,$$

where

$$\begin{aligned} a_1 &= \frac{r_C P_C^*}{K_C} + \mu_C(1-\mathscr{R}_1) \\ a_2 &= b_C \xi_C A_C^* P_C^* + \frac{r_C P_C^*}{K_C}\mu_C(1-\mathscr{R}_1) + \frac{\theta_C \psi_C \omega_C P_C^* I_C^*}{(\omega_C + P_C^*)^2} \\ a_3 &= b_C \xi_C A_C^* P_C^* \mu_C (1-\mathscr{R}_1). \end{aligned}$$

We now apply Routh-Hurwitz criterion to show that the steady state is locally asymptotically stable. Coefficients a_1, a_2, and a_3 are positive if $\mathscr{R}_1 < 1$ and if $\mathscr{R}_2 > 1$ (the latter ensures that A_C^* used in a_2 and a_3 is positive). Observe

$$a_1 a_2 = \frac{r_C P_C^*}{K_C} a_2 + a_3 + \mu_C(1-\mathscr{R}_1)\left(\frac{r_C P_C^*}{K_C}\mu_C(1-\mathscr{R}_1) + \frac{\theta_C \psi_C \omega_C P_C^* I_C^*}{(\omega_C + P_C^*)^2}\right) > a_3.$$

All of the conditions for Routh-Hurwitz Criterion are satisfied which implies that the roots of the characteristic equation have negative real parts. This completes our proof. □

Appendix B The numerical scheme

For the epidemiological model, we approximate solutions to the age structured PDE model with the stored within-host calculations. Let $0 \le t \le T$ be the time interval of interest and $\{t_k\}_{k=1}^n$ be a partition of the time interval with fixed mesh size $\Delta t = T/n$. Let $c_\ell^k = c(\hat{\tau}_\ell, t_k)$ and $i_j^k = i(\tau_j, t_k)$. Let $F^k = F(t_k)$ for all $F \in \{M, S, C, I, R, N\}$.

The numerical scheme a mixed implicit-explicit scheme and is as follows:

$$
\begin{aligned}
i_{j+1}^{k+1} &= \frac{i_j^k}{1+\Delta t(\gamma_{j+1}+d)} \\
c_{\ell+1}^{k+1} &= \frac{c_\ell^k}{1+\Delta t(\alpha_{\ell+1}+d)} \\
R^{k+1} &= \frac{\Delta t^2(1-\rho)\sum_{j=0}^{L-1}\gamma_{j+1}i_{j+1}^{k+1} + \Delta t^2\sum_{\ell=0}^{\hat{L}-1}\alpha_{\ell+1}c_{\ell+1}^{k+1} + R^k}{1+d\Delta t} \\
M^{k+1} &= \frac{\Lambda\Delta t\left(R^{k+1}+\sum_{\ell=0}^{\hat{L}-1}c_{\ell+1}^{k+1}\Delta t\right)\left(1-\frac{N^k}{K}\right)+M^k}{1+\Delta t(d+w)} \\
S^{k+1} &= \frac{\Lambda\Delta t^2\left(1-\frac{N^k}{K}\right)\sum_{j=0}^{L-1}i_{j+1}^{n+1} + wM^{k+1}\Delta t + S^k}{1-\Lambda\Delta t\left(1-\frac{N^k}{K}\right)+\Delta t^2\left(\sum_{j=0}^{L-1}\beta_{j+1}i_{j+1}^{k+1}+\sum_{\ell=0}^{\hat{L}-1}\beta_{C,\ell+1}c_{\ell+1}^{k+1}\right)+d\Delta t} \\
c_0^{k+1} &= \rho\sum_{j=0}^{L-1}\gamma_{j+1}i_{j+1}^{k+1}\Delta t \\
i_0^{k+1} &= S^{k+1}\left(\sum_{j=0}^{L-1}\beta_{j+1}i_{j+1}^{k+1}\Delta t+\sum_{\ell=0}^{\hat{L}-1}\beta_{C,\ell+1}c_{\ell+1}^{k+1}\Delta t\right) \\
N^{k+1} &= S^{k+1}+M^{k+1}+C^{k+1}+I^{k+1}+R^{k+1}
\end{aligned}
$$

where n, L, and $\hat{L}$ are chosen large enough to where $\Delta t = \Delta\tau = \Delta\hat{\tau}$.

Appendix C Sensitivity analysis

The elasticity or normalized forward sensitivity index of a quantity of interest (QOI) q (in our case, q is $\mathcal{R}_0$ for the original system (8)) to a parameter of interest (POI) p (such as immunological scale parameter viral growth rate r_A) can be defined as the ratio of relative change in the variable to the relative change in the parameter:

$$\gamma_p^q = \frac{\partial q}{\partial p} \times \frac{p}{q}.$$

This approach can be implemented across the scales for different QOIs by defining linking functional forms. Through the linking functions appearing in the construction of $\mathcal{R}_0$, $\mathcal{R}_0$ depends implicitly on the within-host state variables. Let p be some parameter used in the within-host model for an infectious individual during the acute

phase. The partial derivative of $\mathcal{R}_0$ with respect to the within-host parameter p is the following:

$$\begin{aligned}\frac{\partial \mathcal{R}_0}{\partial p} &= \hat{S}_0 \int_0^\infty \left(\frac{\partial \beta(\tau,p)}{\partial p} \pi(\tau,p) + \beta(\tau,p) \frac{\partial \pi(\tau,p)}{\partial p} \right) \mathrm{d}\tau \\ &\quad + \hat{S}_0 \rho \int_0^\infty \left(\frac{\partial \gamma(\tau,p)}{\partial p} \pi(\tau,p) + \gamma(\tau,p) \frac{\partial \pi(\tau,p)}{\partial p} \right) \mathrm{d}\tau \int_0^\infty \beta_C(\hat{\tau}) \pi_C(\hat{\tau}) \, \mathrm{d}\hat{\tau},\end{aligned} \tag{C9}$$

where

$$\frac{\partial \beta(\tau,p)}{\partial p} = \frac{2B_0 B_A P(\tau,p) \frac{\partial P(\tau,p)}{\partial p}}{(B_0 + P^2(\tau,p))^2}, \tag{C10a}$$

$$\frac{\partial \gamma(\tau,p)}{\partial p} = \frac{G_A \frac{\partial A(\tau,p)}{\partial p} (P(\tau,p) + \epsilon_0) - G_A A(\tau,p) \frac{\partial P(\tau,p)}{\partial p}}{[P(s,p) + \epsilon_0]^2}, \tag{C10b}$$

$$\frac{\partial \pi(\tau,p)}{\partial p} = -\pi(\tau,p) \int_0^\tau \left(\frac{G_A \frac{\partial A(s,p)}{\partial p} (P(s,p) + \epsilon_0) - G_A A(s,p) \frac{\partial P(s,p)}{\partial p}}{[P(s,p) + \epsilon_0]^2} \right) \mathrm{d}s. \tag{C10c}$$

Let $\hat{p}$ be some parameter used in the within-host model for an infected individual during the carrier phase. The partial derivative of $\mathcal{R}_0$ with respect to the within-carrier parameter $\hat{p}$ is as follows:

$$\frac{\partial \mathcal{R}_0}{\partial \hat{p}} = \hat{S}_0 \rho \int_0^\infty \gamma(\tau) \pi(\tau) \, \mathrm{d}\tau \int_0^\infty \left(\frac{\partial \beta_C(\hat{\tau},\hat{p})}{\partial \hat{p}} \pi_C(\hat{\tau},\hat{p}) + \beta_C(\hat{\tau},\hat{p}) \frac{\partial \pi_C(\hat{\tau},\hat{p})}{\partial \hat{p}} \right) \mathrm{d}\hat{\tau}, \tag{C11}$$

where

$$\frac{\partial \beta_C(\hat{\tau},\hat{p})}{\partial \hat{p}} = \frac{2B_0 B_C P_T(\hat{\tau},\hat{p}) \frac{\partial P_T(\hat{\tau},\hat{p})}{\partial \hat{p}}}{(B_0 + P_T^2(\hat{\tau},\hat{p}))^2}, \tag{C12a}$$

$$\frac{\partial \pi_C(\hat{\tau},\hat{p})}{\partial \hat{p}} = -\pi_C(\hat{\tau},\hat{p}) \int_0^{\hat{\tau}} G_C \frac{\frac{\partial A_C(s,\hat{p})}{\partial \hat{p}} [P_C(s,\hat{p}) + P_T(s,\hat{p}) + \hat{\epsilon}_0] - A_C(s,\hat{p}) \left[\frac{\partial P_C(s,\hat{p})}{\partial \hat{p}} + \frac{\partial P_T(s,\hat{p})}{\partial \hat{p}} \right]}{[P_C(s,\hat{p}) + P_T(s,\hat{p}) + \hat{\epsilon}_0]^2} \mathrm{d}s. \tag{C12b}$$

Observe that we need to compute $\frac{\partial \boldsymbol{x}(\tau,p)}{\partial p}$ and $\frac{\partial \boldsymbol{y}(\hat{\tau},\hat{p})}{\partial \hat{p}}$ where $\boldsymbol{x}(\tau,p) = (I_A(\tau,p), P(\tau,p), A(\tau,p))$ and $\boldsymbol{y}(\hat{\tau},\hat{p}) = (P_T(\hat{\tau},\hat{p}), I_C(\hat{\tau},\hat{p}), P_C(\hat{\tau},\hat{p}), A_C(\hat{\tau},\hat{p}))$. By Clairaut's Theorem, we have that

$$\frac{\partial}{\partial \tau} \left(\frac{\partial \boldsymbol{x}}{\partial p} \right) = \frac{\partial}{\partial p} \left(\frac{\partial \boldsymbol{x}}{\partial \tau} \right) \tag{C13}$$

$$\frac{\partial}{\partial \hat{\tau}} \left(\frac{\partial \boldsymbol{y}}{\partial \hat{p}} \right) = \frac{\partial}{\partial \hat{p}} \left(\frac{\partial \boldsymbol{y}}{\partial \hat{\tau}} \right) \tag{C14}$$

where $\partial \boldsymbol{x}/\partial \tau$ is the right hand side of system (1) and $\partial \boldsymbol{y}/\partial \hat{\tau}$ is the right-hand side of system (2). Let $\boldsymbol{f}(\boldsymbol{x},p) = \partial \boldsymbol{x}/\partial \tau$, and consider the following system for the derivatives $\partial \boldsymbol{x}/\partial p$:

$$\begin{cases} \frac{\partial}{\partial \tau} \left(\frac{\partial \boldsymbol{x}}{\partial p} \right) = \frac{\partial \boldsymbol{f}}{\partial \boldsymbol{x}} \frac{\partial \boldsymbol{x}}{\partial p} + \frac{\partial \boldsymbol{f}}{\partial p}, \\ \frac{\partial \boldsymbol{x}}{\partial p}(0) = \boldsymbol{0}, \end{cases} \tag{C15}$$

where $\partial \boldsymbol{f}/\partial \boldsymbol{x}$ is the Jacobian matrix of the right-hand side of the system (1). We find the solutions for $\boldsymbol{x}$ and the derivatives $\partial \boldsymbol{x}/\partial p$ at all times τ, by solving the extended system (C15)-(1) and we use these solutions to estimate the integrands used in (C9) and (C12b). To numerically solve extended system (C15)-(1), we use ode45 with mesh size set to being 0.01. Additionally, we have the relative and absolute error tolerances for the ODE solver set to being 10^{-10} and 10^{-11}, respectively. For approximating the integrals used in (C9) and (C12b), we use trapezoidal rule.

We incorporate the same techniques for finding $\partial \boldsymbol{y}/\partial \hat{p}$. Let $\boldsymbol{g}(\boldsymbol{y}, \hat{p}) = \partial \boldsymbol{y}/\partial \hat{\tau}$ and consider the following system:

$$\begin{cases} \frac{\partial}{\partial \hat{\tau}} \left(\frac{\partial \boldsymbol{y}}{\partial \hat{p}} \right) = \frac{\partial \boldsymbol{g}}{\partial \boldsymbol{y}} \frac{\partial \boldsymbol{y}}{\partial \hat{p}} + \frac{\partial \boldsymbol{g}}{\partial \hat{p}}, \\ \frac{\partial \boldsymbol{y}}{\partial \hat{p}}(0) = \mathbf{0}, \end{cases} \tag{C16}$$

with $\partial \boldsymbol{g}/\partial \boldsymbol{y}$ is the Jacobian matrix of the right-hand side of the system (2).

Here are a few biological assumptions implemented in the numerical computation of SA:

- *In numerically computing in (C9) and (C12b), the approximated limits of integration that are used for integrals associated with the acute phase is* 0 *and* 30*. Observe in Figure 2, the pathogen load clears well before day 30 and the adaptive immune response is already stabilizing to a fixed value by day 30. For integrals associated with the carrier phase, we use 30 and 750 as our lower and upper bounds of integrals.*
- *The initial conditions used for the within-carrier model are the same values as the ones that are used for acute phase, which leads to a re-simulation of an acute phase. In our previous simulations of the multiscale model we ignore the first τ_* days of the carrier phase (where τ_* is the time for which the pathogen load in the bloodstream $P_C(\tau_*) < 10^{-4}$); however, for the sensitivity analysis experiments, we ignore the first thirty days of the carrier phase since the 28-30 day mark (post infection) is often considered as being the conventional start time of the carrier phase (Stenfeldt C, 2020). Additionally, we observe that in varying some of the within-carrier parameter values (in particular parameters ν, K_C, r_C, δ), we have earlier instances of viral relapse during the carrier phase (in which case τ_* cannot be numerically obtained). We provide plots of these instances in Figure 10. Viral relapse is also observed in generated experimental data, used for the study Macdonald et al. (2022). The computed $\mathcal{R}_0$ value at the baseline parameters is 21.8516.*

Appendix D Additional figures

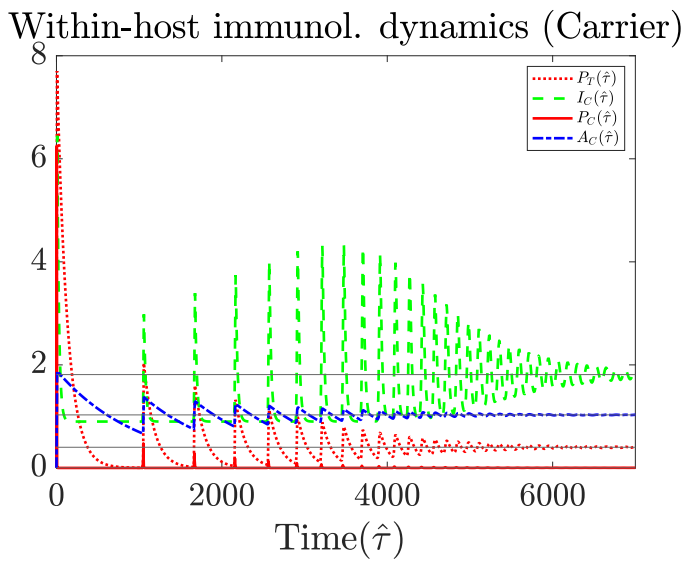

Fig. 11: The within-carrier host dynamics over a 7000 days to further illustrate how the solution to the within-carrier model is converging to the pathogen-persisting interior equilibrium.

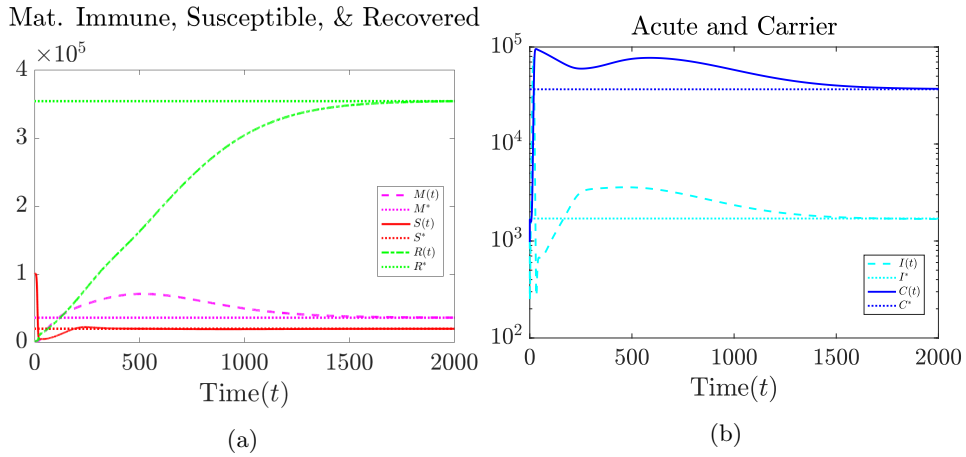

Fig. 12: Between-Host Plots. **Left.** Logarithmic plots of classes $M(t)$, $S(t)$, and $R(t)$, along with the steady states. **Right.** Logarithmic plots of classes $I(t)$ and $C(t)$, along with a plot of the numbers $I^* = \int_0^{\tau_{end}} i^*(0)\pi(\tau)\,\mathrm{d}\tau$ and $C^* = \int_{\tau_*}^{\hat{\tau}_{end}} c^*(0)\pi_C(\hat{\tau})\,\mathrm{d}\hat{\tau}$. All parameters used are given in Table 3.

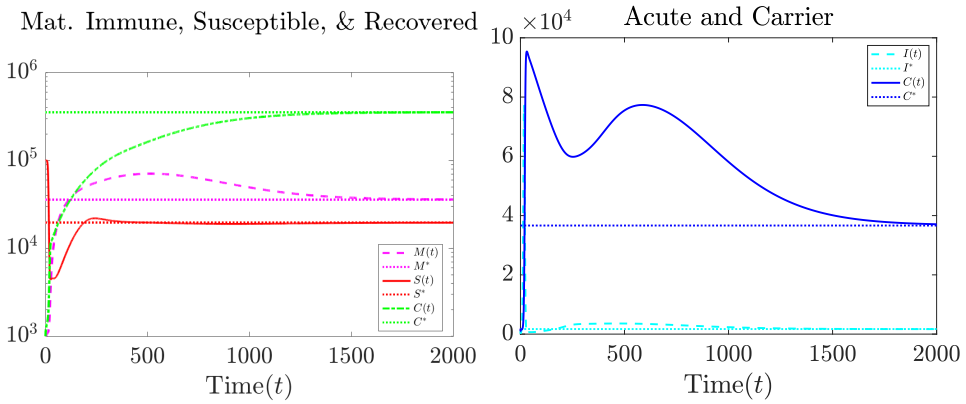

(a) Numerical solution of $M(t)$, $S(t)$, and $R(t)$ and the computed steady states M^*, S^*, and R^*

(b) Numerical solution of $I(t)$ and $C(t)$ and the computed steady states $I^* = \int_0^{\tau_{end}} i^*(0)\pi(\tau)\,\mathrm{d}\tau$ and $C^* = \int_{\tau_*}^{\hat{\tau}_{end}} c^*(0)\pi_C(\hat{\tau})\,\mathrm{d}\hat{\tau}$

Fig. 13: Between-Host Plots along with steady states. **Left.** Plots of classes $M(t)$, $S(t)$, and $R(t)$. **Right.** Plots of classes $I(t)$ and $C(t)$. All parameter values used at given in Table 3.

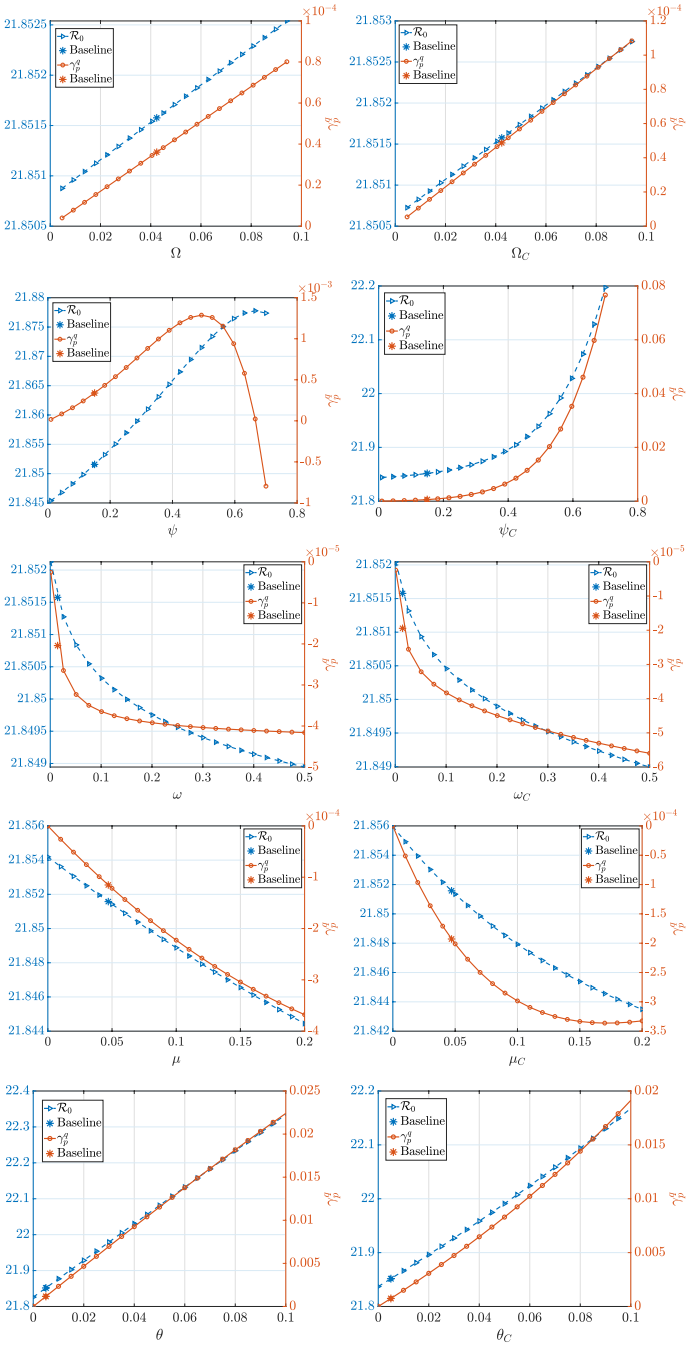

Fig. 14: Sensitivity analysis results. Figures are studying the impact of the innate immune response parameters (Ω, Ω_C, ψ, ψ_C, ω, ω_C,μ, μ_C, θ, θ_C) during acute and carrier stage. We see little change in $\mathcal{R}_0$.

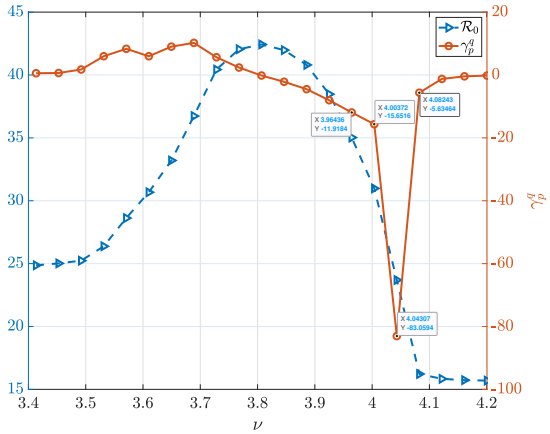

(a) SA results for ν over finer mesh

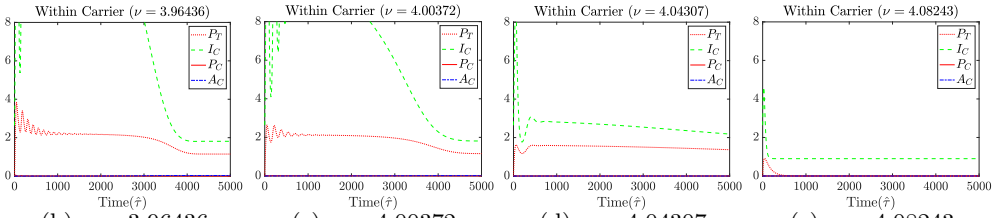

(b) $\nu = 3.96436$ (c) $\nu = 4.00372$ (d) $\nu = 4.04307$ (e) $\nu = 4.08243$

Fig. 15: Sensitivity analysis results of ν alongside the within-carrier solutions to model (2) as described in Figure 9 but displayed over a longer time period. The within-carrier solutions in Figures (b)-(d) are converging to the pathogen persisting equilibrium the solution in Figure (e) is converging to the pathogen-free equilibrium.

References

Garabed, R.B., Jolles, A., Garira, W., Lanzas, C., Gutierrez, J., Rempala, G.: Multi-scale dynamics of infectious diseases. The Royal Society (2020). https://doi.org/10.1098/rsfs.2019.0118

Gloster, J.: Forecasting the airborne spread of foot-and-mouth disease and newcastle disease. Royal Society **302**(111) (1983) https://doi.org/10.1098/rstb.1983.0073

Shikumwifa, E.: Mathematical modeling of foot and mouth disease (fmd) in cattle and buffaloes using vaccination and culling: A namibia perspective. PhD thesis, University of Namibia (2022)

Michel, A.L., Bengis, R.G.: The African buffalo: A villain for inter-species spread of infectious diseases in southern Africa. Onderstepoort Journal of Veterinary Research **79**, 26–30 (2012)

Perez-Martin, E., Beechler, B., Zhang, F., Scott, K., Klerk-Lorist, L.-M., Limon, G., Dugovich, B., Gubbins, S., Botha, A., Hetem, R., *et al.*: Viral dynamics and immune responses to foot-and-mouth disease virus in African buffalo (syncerus caffer). Veterinary research **53**(1), 1–14 (2022)

Stenfeldt C, A.J.: The carrier conundrum; a review of recent advances and persistent gaps regarding the carrier state of foot-and-mouth disease virus. Pathogens **9**(3) (2020) https://doi.org/10.3390/pathogens9030167

Jolles, A., Gorsich, E., Gubbins, S., Beechler, B., Buss, P., Juleff, N., Klerk-Lorist, L.-M., Maree, F., Perez-Martin, E., Schalkwyk, O.L., Scott, K., Zhang, F., Medlock, J., Charleston, B.: Endemic persistence of a highly contagious pathogen: Foot-and-mouth disease in its wildlife host. Science **374**(6563), 104–109 (2021) https://doi.org/10.1126/science.abd2475 https://www.science.org/doi/pdf/10.1126/science.abd2475

Pech, R.P., McIlroy, J.: A model of the velocity of advance of foot and mouth disease in feral pigs. Journal of Applied Ecology, 635–650 (1990)

Chowell, G., Rivas, A.L., Hengartner, N.W., Hyman, J.M., Castillo-Chavez, C.: The role of spatial mixing in the spread of foot-and-mouth disease. Preventive Veterinary Medicine **73**(4), 297–314 (2006) https://doi.org/10.1016/j.prevetmed.2005.10.002

Gashirai, T.B., Musekwa-Hove, S.D., Lolika, P.O., Mushayabasa, S.: Global stability and optimal control analysis of a foot-and-mouth disease model with vaccine failure and environmental transmission. Chaos, Solitons & Fractals **132**, 109568 (2020)

Hayer, S., VanderWaal, K., Ranjan, R., Biswal, J., Subramaniam, S., Mohapatra, J., Sharma, G., Rout, M., Dash, B., Das, B., *et al.*: Foot-and-mouth disease virus transmission dynamics and persistence in a herd of vaccinated dairy cattle in india.

Transboundary and emerging diseases **65**(2), 404–415 (2018)

McLachlan, I., Marion, G., McKendrick, I.J., Porphyre, T., Handel, I.G., Bronsvoort, B.M.: Endemic foot and mouth disease: pastoral in-herd disease dynamics in sub-saharan africa. journal **volume**(number) (2019) https://doi.org/10.1038/s41598-019-53658-5

Howey, R., Quan, M., Savill, N.J., Matthews, L., Alexandersen, S., Woolhouse, M.: Effects of the initial dose of foot-and-mouth disease virus on the early viral dynamics within pigs. Journal of the Royal Society Interface **6**, 835–847 (2009)

Howey, R., Bankowski, B., Juleff, N., Savill, N.J., Gibson, D., Fazakerley, J., Charleston, B., Woolhouse, M.E.J.: Modelling the within-host dynamics of the foot-and-mouth disease virus in cattle. Epidemics **4**, 93–103 (2012)

Macdonald, J.C., Gulbudak, H., Beechler, B., Gorsich, E., Gubbins, S., Perez-Martin, E., Jolles, A.: Consilience in disease ecology: FMDV transmission dynamics reflect viral growth and immune response rates. bioRxiv, 2022–12 (2022)

Bradhurst, R.A., Roche, S.E., East, I.J., Kwan, P., Garner, M.G.: A hybrid modeling approach to simulating foot-and-mouth disease outbreaks in australian livestock. Frontiers in Environmental Science **3**, 17 (2015)

Ferguson, N.M., Donnelly, C.A., Anderson, R.M.: The foot-and-mouth epidemic in great britain: Pattern of spread and impact of interventions. Science **292**(5519), 1155–1160 (2001) https://doi.org/10.1126/science.1061020 https://www.science.org/doi/pdf/10.1126/science.1061020

Hayama, Y., Yamamoto, T., Kobayashi, S., Muroga, N., Tsutsui, T.: Mathematical model of the 2010 foot-and-mouth disease epidemic in japan and evaluation of control measures. Preventive Veterinary Medicine **112**(3), 183–193 (2013) https://doi.org/10.1016/j.prevetmed.2013.08.010

Keeling, M.J., Woolhouse, M.E.J., Shaw, D.J., Matthews, L., Chase-Topping, M., Haydon, D.T., Cornell, S.J., Kappey, J., Wilesmith, J., Grenfell, B.T.: Dynamics of the 2001 uk foot and mouth epidemic: Stochastic dispersal in a heterogeneous landscape. Science **294**(5543), 813–817 (2001) https://doi.org/10.1126/science.1065973 https://www.science.org/doi/pdf/10.1126/science.1065973

Tildesley, M.J., Savill, N.J., Shaw, D.J., Deardon, R., Brooks, S.P., Woolhouse, M.E.J., Grenfell, B.T., Keeling, M.J.: Optimal reactive vaccination strategies for a foot-and-mouth outbreak in the uk. Nature **440**(7080), 83–86 (2006) https://doi.org/10.1038/nature04324

Michael J. Tildesley, M.J.K. Paul R. Bessell, Woolhouse, M.E.J.: The role of pre-emptive culling in the control of foot-and-mouth disease. The Royal Society (2009) https://doi.org/10.1098/rspb.2009.0427

Thomson, G.R., Vosloo, W., Esterhuysen, J.J., Bengis, R.G.: Maintenance of foot and mouth disease viruses in buffalo (syncerus caffer sparrman, 1779) in southern africa. Rev Sci Tech. **11**(4), 1097–1097 (1992)

Juleff, N., Windsor, M., Reid, E., Seago, J., Zhang, Z., Monaghan, P., Morrison, I.W., Charleston, B.: Foot-and-mouth disease virus persists in the light zone of germinal centres. PloS one **3**(10), 3434 (2008)

Maree, F., Klerk-Lorist, L.-M., Gubbins, S., Zhang, F., Seago, J., Pérez-Martín, E., Reid, L., Scott, K., Schalkwyk, L., Bengis, R., *et al.*: Differential persistence of foot-and-mouth disease virus in african buffalo is related to virus virulence. Journal of virology **90**(10), 5132–5140 (2016)

Gulbudak, H., Qu, Z., Milner, F., Tuncer, N.: Sensitivity analysis in an immuno-epidemiological vector-host model. Bull Math Biol **84**(27) (2022) https://doi.org/10.1007/s11538-021-00979-0

Handel, A., Rohani, P.: Crossing the scale from within-host infection dynamics to between-host transmission fitness: a discussion of current assumptions and knowledge. Philosophical Transactions of the Royal Society B: Biological Sciences **370** (2015)

Fraser, C., Lythgoe, K., Leventhal, G.E., Shirreff, G., Hollingsworth, T.D., Alizon, S., Bonhoeffer, S.: Virulence and pathogenesis of HIV-1 infection: an evolutionary perspective. Science **343**(6177), 1243727 (2014) https://doi.org/10.1126/science.1243727

Gulbudak, H., Cannataro, V.L., Tuncer, N., Martcheva, M.: Vector-borne pathogen and host evolution in a structured immuno-epidemiological system. Bulletin of Mathematical Biology **79** (2017) https://doi.org/10.1007/s11538-016-0239-0

Gilchrist, M., Sasaki, A.: Modeling host–parasite coevolution: A nested approach based on mechanistic models. Journal of Theoretical Biology **218**(3) (2002)

Gulbudak, H., Browne, C.J.: Infection severity across scales in multi-strain immuno-epidemiological dengue model structured by host antibody level. Journal of Mathematical Biology **80**(6) (2020) https://doi.org/10.1007/s00285-020-01480-3

Tuncer, N., Gulbudak, H., Cannataro, V.L., Martcheva, M.: Structural and practical identifiability issues of immuno-epidemiological vector–host models with application to rift valley fever. Bulletin of Mathematical Biology **78**(9) (2016) https://doi.org/10.1007/s11538-016-0200-2

Barfield, M., Martcheva, M., Tuncer, N., Holt, R.: Backward bifurcation and oscillations in a nested immuno-eco-epidemiological model. Journal of Biological Dynamics **12**(1) (2018) https://doi.org/10.1080/17513758.2017.1401676

Gulbudak, H., Salceanu, P.L., Wolkowicz, G.S.K.: A delay model for persistent viral infections in replicating cells. Journal of Mathematical Biology **59**(82) (2021) https://doi.org/10.1007/s00285-021-01612-3

Gulbudak, H., Martcheva, M.: Forward hysteresis and backward bifurcation caused by culling in an avian influenza model. Mathematical Biosciences **246**(1) (2013) https://doi.org/10.1016/j.mbs.2013.09.001

Welker, J.S., Marcheva, M.: Analysis and simulations with a multi-scale model of canine visceral leishmaniasis. Math. Model. Nat. Phenom. **15**(72) (2020) https://doi.org/10.1051/mmnp/2020026

Grassly, N.C., Fraser, C.: Mathematical models of infectious disease transmission. Nature Reviews Microbiology **6**(6), 477–487 (2008)

Sartwell, P.E.: The distribution of incubation periods of infectious disease. American journal of epidemiology **141**(5), 386–394 (1995)

Fine, P.E.M.: The Interval between Successive Cases of an Infectious Disease. American Journal of Epidemiology **158**(11), 1039–1047 (2003) https://doi.org/10.1093/aje/kwg251 https://academic.oup.com/aje/article-pdf/158/11/1039/385770/kwg251.pdf

Macdonald, J., Gulbudak, H., Beechler, B., Gorsich, E.E., Gubbins, S., Perez-Martin, E., Jolles, A.E.: Experimental data for Consilience in disease ecology: FMDV transmission dynamics reflect viral growth and immune response rates. https://doi.org/10.6084/m9.figshare.21701612.v1 (2022)